

Data-driven learning of feedback maps for explicit robust predictive control: an approximation theoretic view

SIDDHARTHA GANGULY , SHUBHAM GUPTA, DEBASISH CHATTERJEE 

ABSTRACT. We establish an algorithm to learn feedback maps from data for a class of robust model predictive control (MPC) problems. The algorithm accounts for the approximation errors due to the learning directly at the synthesis stage, ensuring recursive feasibility by construction. The optimal control problem consists of a linear noisy dynamical system, a quadratic stage and quadratic terminal costs as the objective, and convex constraints on the state, control, and disturbance sequences; the control minimizes and the disturbance maximizes the objective. We proceed via two steps — **(a) Data generation:** First, we reformulate the given minmax problem into a convex semi-infinite program and employ recently developed tools to solve it in an *exact* fashion on grid points of the state space to generate (state, action) data. **(b) Learning approximate feedback maps:** We employ a couple of approximation schemes that furnish tight approximations within preassigned *uniform* error bounds on the admissible state space to learn the unknown feedback policy. The stability of the closed-loop system under the approximate feedback policies is also guaranteed under a standard set of hypotheses. Two benchmark numerical examples are provided to illustrate the results.

1. Introduction

This article tackles the problem of learning constrained feedback policies for robust model predictive control (MPC) of uncertain linear systems using offline data. Specifically, it explores how offline data, which may include historical measurements or pre-collected input-output trajectories, can be leveraged to train a function approximator that generates (approximate) feedback policies for constrained robust optimal control. Once trained offline, the feedback policy is implemented online, where it continuously responds to the system’s states in order to undertake control decisions under constraints in real time. To this end, we focus on the task of performing receding horizon control (RHC), commonly known as model predictive control, in a fast and efficient manner by learning feedback maps/policies from offline data (hence, data-driven) with uniform approximation guarantees.

MPC [XL19] is a dynamic optimization/optimal control technique for synthesizing constrained feedback control that has been successfully applied across an array of industries including electrical [BVP⁺12], robotics and trajectory generation [KSAS17, GDC24],

Date: 16th October 2025 12:55am GMT.

2020 Mathematics Subject Classification. 49N35, 93B51, 93B52, 90C34, 62M45, 41A05.

Key words and phrases. Robust optimal control, feedback synthesis, model predictive control, approximation theory, neural networks.

S. Ganguly is with  The Applied Mathematics and Physics Department, Graduate School of Informatics,  Kyoto University,  Kyoto, Japan. S. Gupta is with  Department of Mechanical and Process Engineering  ETH Zurich,  Switzerland. D. Chatterjee is with  Systems & Control Engineering,  IIT Bombay, Powai,  Mumbai 400076, India.

Contact Information: (SG)  <https://sites.google.com/view/siddhartha-ganguly>,  ganguly.siddhartha.7p@kyoto-u.ac.jp. (SuG)  shugupta@ethz.ch. (DC)  <https://www.sc.iitb.ac.in/~chatterjee>,  dchatter@iitb.ac.in.

chemical [MRLSO19], power electronics [CKK⁺08], oil and gas, among several others. The ability to directly integrate constraints into the control design process sets MPC apart from other conventional control techniques; consequently, aggressive control actions are generated and the closed-loop processes tend to operate at the boundary of their admissible regions — an extremely desirable feature in applications.

Let us take a high-level look at the MPC framework: In MPC, the “model” represents a discrete-time controlled dynamical system defined on a Euclidean space, formulated as $x_{t+1} = f(x_t, u_t)$ for all $t \in \mathbb{N}$. Here, for each $t \in \mathbb{N}^*$, x_t and u_t are the state and the control variable, and $f(\cdot, \cdot)$ is a known mapping. Let $U := (u_0, \dots, u_{N-1})$, the MPC method entails solving a constrained optimal control problem (OCP) over a given time horizon $N \in \mathbb{N}^*$, formulated as

$$(P) \quad \begin{aligned} \inf_U & \quad \sum_{t=0}^{N-1} c(x_t, u_t) + c_F(x_N) \\ \text{subject to} & \quad \begin{cases} x_{t+1} = f(x_t, u_t), \quad x_0 := \bar{x}, \quad x_t \in \mathbb{M}, \\ u_t \in \mathbb{U} \text{ for } t \in \{0, \dots, N-1\}, \quad x_N \in \mathbb{M}_F. \end{cases} \end{aligned}$$

In this context, $c(\cdot, \cdot)$ and $c_F(\cdot)$ denote the stage cost and the final (or terminal) cost functions, respectively, while \mathbb{M} , \mathbb{U} , and \mathbb{M}_F define the admissible sets for states, control inputs, and final states, respectively. At $t = 0$, the system’s initial state is observed as $x_0 := \bar{x}$, and the optimization problem is solved with \bar{x} to determine an optimal control sequence $U^* \in \mathbb{U}^N$; notice that \bar{x} enters (P) as a *parameter*. The first control input, u_0^* , is then applied to the system. Time is advanced to $t = 1$, and the process is repeated iteratively. This iterative approach inherently defines a *feedback map* (potentially set-valued), as the control action $\bar{x} \mapsto u_0^*(\bar{x})$ implicitly depends on the current state \bar{x} . The goal of **Explicit MPC** (ExMPC) is to computationally extract this *implicit* map [WHL22]. The ExMPC approach is particularly valuable as it replaces the need for repeated numerical optimization in the MPC problem with a simple function evaluation at each state. This eliminates the necessity of solving the OCP (P) at every time step via shifting the time horizon, significantly reducing computational overhead for real-time applications. Consequently, ExMPC is well-suited for a variety of industrial process applications [MDM12], [CKK⁺08]. Most existing ExMPC methods rely on multiparametric programming [XL19, Chapter 7], but their applicability is largely confined to nominal linear, low-dimensional systems with short time horizons. For systems with moderate to high dimensionality, neural networks have been utilized to develop ExMPC algorithms, as seen in earlier works like [PZ95] and more recent advancements such as [PM20, WHL22, WWTW24, WZW⁺24, KL20, WCW⁺24]. Although some of these approaches offer NN-based ExMPC methods with closed-loop guarantees, they all fail to adequately address the challenges of approximation errors or provide strategies for controlling them, even in low-dimensional settings.

While ExMPC, has become standard for nominal linear models, accounting for uncertainty in the systems introduces a fresh complication into the problem — in particular, (P) becomes a minmax optimization problem. Robust optimization techniques can in principle be employed to ensure that the MPC policy becomes immune to a range of model uncertainties, but this is easier said than done due to the intrinsic difficulties associated with numerical solutions of robust optimization problems.

Our contributions.

- A. **Approximation-aware formulation:** We present a numerically tractable technique to learn explicit feedback policies for a class of MPC problems with uniform approximation error guarantees. As a first step, one of our key contributions is the formulation of an *approximation-aware* MPC setup that yields a policy that respects all constraints

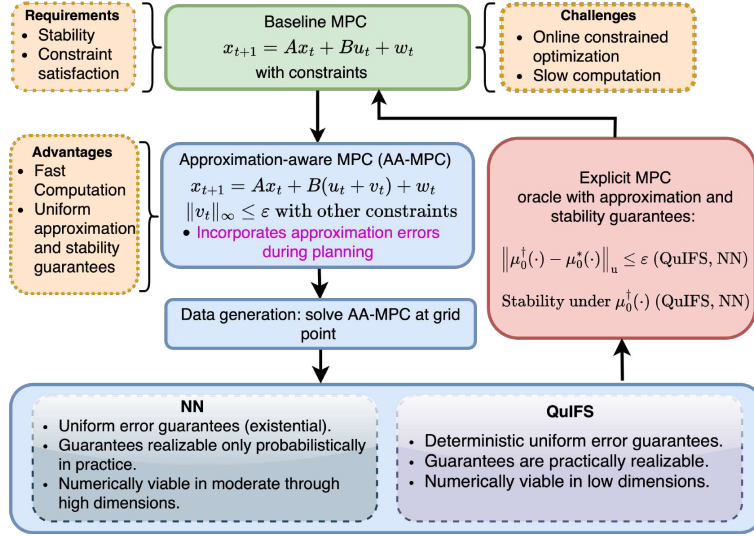


Figure 1. A bird's-eye view of our algorithm and its main components.

by design irrespective of approximation errors, thereby ensuring recursive feasibility and closed-loop stability. This is a clear point of departure from the existing literature that mostly provides providing a posteriori error bounds without taking such errors into account at the planning stage.

- We build our theoretical results around a robust constrained MPC framework for an uncertain discrete-time linear dynamical system, where we explicitly account for the error arising due to the application of the approximate policy $\bar{x} \mapsto \mu_0^\dagger(\bar{x})$ instead of the (optimal) MPC policy $\bar{x} \mapsto \mu_0^*(\bar{x})$, and robustify against that error. Here we introduce the *approximation-aware* MPC problem: For this problem to be well-posed, it is essential to ensure a *uniform* approximation error between the optimal policies $\mu_0^*(\cdot)$ and its approximants $\mu_0^\dagger(\cdot)$. The algorithms established in the sequel inherently address this requirement.
- The synthesis of the approximate policies relies on interpolation and learning techniques, and three attributes of this procedure are central:
 - (T-a)** the ability to guarantee uniform approximation within a preassigned error margin;
 - (T-b)** a training procedure that produces such an approximant, and
 - (T-c)** numerical viability.

We explore two learning engines in this context: quasi-interpolation and neural networks. For a prespecified uniform error tolerance $\varepsilon > 0$, our quasi-interpolation driven procedure satisfies all the three attributes **(T-a)–(T-c)** for low-dimensional systems (at most $d = 5$); the neural network driven procedure checks the first attribute under abundance of training data but the second attribute is difficult to ensure in practice as we shall demonstrate via numerical experiments. There is, however, reason to stay cautiously optimistic concerning the applicability of neural networks, as we point out in the sequel.

B. A semi-infinite programming-based method for exact (state, action) data generation: The underlying dynamical system in our framework is an *uncertain linear system*, where the robust MPC problem is formulated as a worst-case minmax optimization. The (outer) minimization is performed over a class of control policies, while

the (inner) maximization considers all admissible uncertainties, subject to convex constraints. The ensuing convex robust optimization problem is, in general, NP-hard. However, a recently-developed technique [DACC22] for *exact* solutions to convex semi-infinite programs (which we refer to as the MSA algorithm in the sequel) are employed herein to solve this important class of robust MPC problems in an *exact* fashion at specific grid points on the state space; we submit that this approach leads to the extraction of accurate optimizers for any feasible initial state.¹ Moreover, due to the absence of conservative approximations, *the exact feasible set* of the minmax problem is larger than those obtained via conservative approximations; see Example 4.1 in §4 for an illustration.² We draw attention to the fact that alternative techniques such as the scenario approach for solving the minmax problem may suffer, especially in high dimensions, from acute suboptimality issues highlighted in [ACB20, Section 1.5] and [DACC22, Remark 12], which are circumvented via the MSA algorithm.³ Our results concerning this contribution are recorded in §3.1.

The issue of computing the exact optimizers for the underlying minmax problem at each given initial state is addressed by the MSA algorithm, but the algorithm is typically slow (due to the presence of a global optimization step therein). Consequently, a direct online application may not be possible always, and that brings us to our second key contribution by means of function learning:

C. Approximation/learning feedback maps from data: Instead of computing control actions through optimization at each step, we learn a feedback map to evaluate them, but with a twist. In contrast to the standard approaches we advocate *tight approximations* of the underlying implicit feedback for the construction of the explicit map; this approximation is driven by means of input-output data of the form (state, action)-pairs made available by the MSA algorithm. Only uniformly approximate designs can be utilized in this context for operational reasons (see Remark 2.1 for a detailed discussion), and we submit two approaches for learning such uniformly approximate explicit feedback maps:

- (a) Along the lines of the QuIFS algorithm reported in [GC25], the first approach applies to low-dimensional systems and employs *quasi-interpolation* to learn continuous functions from the (state, action) data on a uniform cardinal grid up to a *preassigned uniform error*. For engineers, this paradigm is extremely well-suited, and works well in the robust MPC context. The designer specifies an error tolerance $\varepsilon > 0$ and selects a rapidly decaying smooth generating/basis function $\psi(\cdot)$ along with three parameters $(h, \mathcal{D}, \rho) \in]0, +\infty[^3$ such that the error between the optimal and learned feedback policies remains within ε *uniformly* over the admissible set. The *uniformity* in the estimate permits us to accommodate, with foresight, this (small) error into the minmax formulation itself so that recursive feasibility is not compromised at any stage and the closed-loop robust stability is ensured. Our results corresponding to this approach are reported in §3.2 – §3.3.
- (b) The presence of a uniform cardinal grid on the feasible set in C.a limits this interpolation-based technique to low state dimensions. For moderate-dimensional systems, recent results regarding uniform approximation properties of deep neural networks [SYZ22] point to an alternative approach to learn an approximate (and sometimes theoretically the *exact*) explicit feedback map based on the offline

¹See §A.2 in Appendix A for a brief overview of the MSA algorithm.

²This example demonstrates that the feasible set of initial points \bar{x} obtained using our method is strictly larger compared to the feasible set obtained by employing YALMIP’s [Löf04] robust optimization module [Löf12] which employs scenario-like approximation methods.

³The MSA algorithm is not limited to quadratic costs and linear constraints; while certain specific structures of minmax problems may be solvable by alternate means, MSA offers a general framework that applies to all minmax problems of the “convex” type — see [DACC22] for details.

precomputed (state, action) data (in this regime either on a uniform cardinal grid or on a suitably randomly sampled set of points as the case may be) via training an appropriate neural network (in our case, a deep ReLU network [DHP21]). To fulfill the requirement **(T-a)–(T-b)** numerically, our empirical results demonstrate that there are reasons to be cautiously optimistic even though the *current* state-of-the-art theoretical requirements are prohibitive from a numerical tractability standpoint. The results corresponding to this approach are reported in §3.4 – §3.5.

Notation: We let $\mathbb{N}^* := \{1, 2, \dots\}$ denote the set of positive integers, $\mathbb{N} := \mathbb{N}^* \cup \{0\}$, and let \mathbb{Z} denote the integers. Let $\hat{a}, \bar{a} \in \mathbb{N}^*$ and $\bar{a} > \hat{a}$, then $[\hat{a}; \bar{a}] := \{\hat{a}, \hat{a} + 1, \dots, \bar{a}\}$. The vector space \mathbb{R}^d is assumed to be equipped with standard inner product $\langle v, v' \rangle := \sum_{j=1}^d v_j v'_j$ for every $v, v' \in \mathbb{R}^d$. For any arbitrary subset $X \subset \mathbb{R}^d$ we denote the interior of X by $\text{int } X$. The notation \oplus is the standard Minkowski sum of two sets. We denote the uniform function norm via the notation $\|\cdot\|_u$; more precisely, for a real-valued bounded function $f(\cdot)$ defined on a set S , it is given by $\|f(\cdot)\|_u := \sup_{x \in S} |f(x)|$. For vectors residing in some finite dimensional vector space \mathbb{R}^d we employ the notation $\|\cdot\|_\infty$ for uniform norm. For $\ell \in \mathbb{N}^*$ and for $p \in [1, +\infty]$, the ℓ -dimensional closed ball centered at x and of radius $\eta > 0$ with respect to the p -norm (vector) is denoted by $B_p^\ell[x, \eta]$; $\Gamma(\cdot)$ will denote the standard Gamma function. The Schwartz space of rapidly decaying \mathbb{R} -valued functions [MS07, Chapter 2] on \mathbb{R}^d is denoted by $\mathcal{S}(\mathbb{R}^d)$.

2. Problem formulation

Consider a time-invariant discrete-time control system

$$(1) \quad x_{t+1} = Ax_t + Bu_t + w_t, \quad x_0 = \bar{x} \text{ given,} \quad t \in \mathbb{N},$$

along with the following data:

- (1-a) $x_t \in \mathbb{R}^d$, $u_t \in \mathbb{R}^m$, and $w_t \in \mathbb{R}^d$ are the vectors representing the states, control inputs and uncertainties at the time t , with $A \in \mathbb{R}^{d \times d}$ and $B \in \mathbb{R}^{d \times m}$;
- (1-b) the constraints on the state and control inputs of the system (1) are given by $x_t \in \mathbb{M}$ and $u_t \in \mathbb{U}$ for all $t \in \mathbb{N}$, where $\mathbb{M} \subset \mathbb{R}^d$ and $\mathbb{U} \subset \mathbb{R}^m$ are nonempty compact and convex subsets both containing the origins $0 \in \mathbb{R}^d$ and $0 \in \mathbb{R}^m$ in their respective interiors. The vector w_t represents the uncertainty entering in the system at each time t and $w_t \in \mathbb{W}$ for all $t \in \mathbb{N}$, where $\mathbb{W} \subset \mathbb{R}^d$ is a nonempty compact and convex with origin $0 \in \mathbb{R}^d$ in its interior.

We assume that the following objects are given:

- (1-c) a time horizon $N \in \mathbb{N}^*$; a jointly continuous and convex *cost-per-stage* function $c(\cdot, \cdot)$ and a continuous and convex *final-stage cost* function $c_F(\cdot)$ satisfying $c(0, 0) = 0$ and $c_F(0) = 0$;
- (1-d) a closed and convex terminal set $\mathbb{M}_F \subset \mathbb{M}$ containing the origin $0 \in \mathbb{R}^d$ in its interior; a class of admissible control policies Π consisting of a sequence $\pi(\cdot) := (\pi_t(\cdot))_{t=0}^{N-1}$ of continuous maps such that $\pi_t : \mathbb{M} \rightarrow \mathbb{U}$ for each t and we write $u_t = \pi_t(x_t)$.

Let $w := (w_t)_{t=0}^{N-1}$. Given the preceding set of data, the **baseline robust MPC problem (BL-MPC)** for the system (1) accompanied by the data (1-a)-(1-d) is:

$$(2) \quad \begin{aligned} \inf_{\pi(\cdot)} \sup_w \quad & \mathbb{J}_N(\bar{x}, \pi(\cdot), w) := \sum_{t=0}^{N-1} c(x_t, u_t) + c_F(x_N) \\ \text{subject to} \quad & \begin{cases} \text{dynamics (1), } x_0 = \bar{x}, u_t = \pi_t(x_t), \\ x_N \in \mathbb{M}_F, x_t \in \mathbb{M} \text{ and } u_t \in \mathbb{U} \\ \text{for all } (t, w_t) \in [0; N-1] \times \mathbb{W}. \end{cases} \end{aligned}$$

A solution to (2) (if exists) is a control policy $\pi^*(\cdot) := (\pi_t^*(\cdot))_{t=0}^{N-1}$, which, by definition, satisfies all constraints for any disturbance realization. If $\pi^*(\cdot)$ is unique for each $\bar{x} \in \mathbb{M}$ (a parameter of (2)), the mapping from \bar{x} to $\pi^*(\cdot)$ is a function, with $\pi_0^*(\cdot)$ being the *feedback map*. Non-uniqueness results in a set-valued mapping.⁴ Computing the exact $\pi_0^*(\cdot)$ is extremely challenging, as it requires solving the Bellman-Isaacs equation [BB08]. Instead, we adopt an optimization-based approach. Assuming $\pi^*(\cdot)$ can be evaluated at each feasible point, we construct a tight uniform approximation of $\pi_0^*(\cdot)$. Naturally, this introduces approximation errors, which manifest as uncertainties in the control actions and these must be accounted for at the design stage to ensure recursive feasibility, leading to the focus of the next subsection.

2.1. From the (BL-MPC) (2) to the approximation-aware MPC problem. To account for approximation error, we solve an OCP that exhibits several common features with (2) at the level of the cost and the constraints, but differs at the level of the dynamics. To this end, define $\tilde{w}_t := w_t + Bv_t$ which takes values in the set $\tilde{\mathbb{W}} := \mathbb{W} \oplus BB_\infty^m[0, \varepsilon]$ and let $W := (\tilde{w}_0, \dots, \tilde{w}_{N-1}) \in \tilde{\mathbb{W}}^N$. Consider the dynamical system

$$(3) \quad x_{t+1} = Ax_t + Bu_t + \tilde{w}_t, \quad x_0 = \bar{x} \text{ given,} \quad t \in \mathbb{N},$$

where $x_t \in \mathbb{M}$, $u_t \in \mathbb{U}$, and the uncertainly component $(w_t, v_t) \in \mathbb{W} \times B_\infty^m[0, \varepsilon]$ for each $t = 0, \dots, N-1$, where the designer-specified uniform approximation error margin $\varepsilon > 0$ has been fixed *a priori*. The data (1-a)–(1-b) carry over to (3) modulo obvious changes; and the data (1-c)–(1-d) from the baseline MPC problem (2) are satisfied. Our **approximation-aware robust MPC problem (AA-MPC)** for the synthesis of receding horizon feedback is given by

$$(4) \quad \begin{aligned} \inf_{\pi(\cdot)} \sup_W \quad & \mathbb{J}_N(\bar{x}, \pi(\cdot), W) := \sum_{t=0}^{N-1} c(x_t, u_t) + c_F(x_N) \\ \text{subject to} \quad & \begin{cases} \text{dynamics (3), } x_0 = \bar{x}, u_t = \pi_t(x_t), \\ x_N \in \mathbb{M}_F, x_t \in \mathbb{M} \text{ and } u_t + v_t \in \mathbb{U} \\ \text{for all } (t, W) \in [0; N-1] \times \tilde{\mathbb{W}}^N. \end{cases} \end{aligned}$$

REMARK 2.1. The noise $(v_t)_{t \in \mathbb{N}}$ in (3) represents uncertainty in the control action introduced by approximating the optimal feedback in closed-loop. The constraint $\|v_t\|_\infty \leq \varepsilon$ is enforced during the synthesis stage of (4), ensuring all uncertainties in (1) are accounted for. Our learning method depends on the state-space dimension. For low-dimensional systems, we use a grid-based quasi-interpolation technique QuIFL (Quasi-interpolation-based Feedback Learning), while moderate-dimensional systems employ neural network-based approximation NNFL (Neural Network-based Feedback Learning); both furnish uniform approximation guarantees, as detailed in §3.

2.2. From the (AA-MPC) (4) to a convex SIP problem. The (BL-MPC) and the (AA-MPC), i.e., the robust OCPs (2) and (4), in general, are numerically intractable despite being perfectly sensible in theory. For state-feedback parameterization of the control policy, it is well-known that the set of admissible decision variables can turn out to be *non-convex* [Löf03b] in general. We adopt a parameterization employing the past disturbance data instead [Löf03a]

$$(5) \quad u_t = \sum_{i=0}^{t-1} \theta_{t,i} \tilde{w}_i + \eta_t, \quad t = 0, \dots, N-1,$$

⁴See [Don21, Lecture 0, p. 4] for details.

where each $\theta_{t,i} \in \mathbb{R}^{m \times d}$, $\eta_t \in \mathbb{R}^m$, and eliminating (t, i) we have $(\theta, \eta) \in \mathbb{R}^{mN \times dN} \times \mathbb{R}^{mN}$. Employing the parameterization in (5), the problem (4) now reads as

$$(6) \quad \mathbb{J}_N^*(\bar{x}) := \inf_{\theta, \eta} \sup_W \{ \mathbb{J}_N(\bar{x}, \theta, \eta, W) \mid \text{the constraints in (4)} \}.$$

Let the set of feasible decision variables $(\theta, \eta) \in \mathbb{R}^{mN \times dN} \times \mathbb{R}^{mN}$ for the problem (6) is given by $\mathcal{A}_{\theta, \eta}(\bar{x})$. Notice that, for a given initial state \bar{x} , the set $\mathcal{A}_{\theta, \eta}(\bar{x})$ is convex [Löf03b]. This approach allows for the determination of an admissible policy by solving a *convex semi-infinite program*, for a wide range of disturbances and uncertainties.

We define the feasible set of initial states, corresponding to the optimization problem (6) by

$$(7) \quad X_N := \{\bar{x} \in \mathbb{R}^d \mid \mathcal{A}_{\theta, \eta}(\bar{x}) \neq \emptyset\}.$$

ASSUMPTION 2.2. We assume that the set of feasible initial states X_N defined in (7) is nonempty and that the problem (6) admits a unique solution that we denote by $(\mu_t^*(\cdot))_{t=0}^{N-1}$.

The first entry $\mu_0^*(\cdot)$ of the optimal policy $(\mu_t^*(\cdot))_{t=0}^{N-1}$ obtained by solving the OCP (6) is important for us, and for each \bar{x} , the evaluation $\mu_0^*(\bar{x})$ of $\mu_0^*(\cdot)$ at \bar{x} is obtained numerically by solving (6). As mentioned above, before the synthesis process begins, the designer is allowed to fix an error margin, say $\varepsilon > 0$, and, if $\mu_0^\dagger(\cdot)$ is an approximation of $\mu_0^*(\cdot)$, then it is stipulated that the approximation error satisfies

$$(8) \quad \left\| \mu_0^*(\cdot) - \mu_0^\dagger(\cdot) \right\|_{\text{u}} \leq \varepsilon,$$

i.e., $\| \mu_0^*(y) - \mu_0^\dagger(y) \| \leq \varepsilon$ for all feasible $y \in X_N$. Our **learning-based robust feedback control** technique for (1) is encoded in the following two steps:

- (FL1) measure the states x_t at time t ,
- (FL2) apply $u_t = \mu_0^\dagger(x_t)$, increment t to $t + 1$, and repeat.

Since the approximation error uncertainty (8) is accounted for in (6), using $u_t = \mu_0^\dagger(x_t)$ in (1) ensures constraint satisfaction at every stage and recursive feasibility by design. Our learning-based robust feedback control will be implemented via steps (FL1)–(FL2) using the approximate policy $\mu_0^\dagger(\cdot)$. For a streamlined presentation, we use the same notation, $\mu_0^\dagger(\cdot)$, to represent the approximate policy learned through both quasi-interpolation and the neural network architecture.

We now transition towards the numerical technique that we devise herein to solve (6). Consider the problem (6) with its problem data and notations. Introducing a *slack variable* $r \in [0, +\infty[$, the problem (6) can be translated into:

$$(9) \quad \begin{aligned} & \inf_{\theta, \eta, r} && r \\ & \text{subject to} && \begin{cases} \mathbb{J}_N(\bar{x}, \theta, \eta, W) - r \leq 0, r \in [0, +\infty[, \\ \text{the constraints in (4), for all } W \in \tilde{\mathbb{W}}^N \end{cases} \end{aligned}$$

Observe that (9) is a *convex semi-infinite optimization problem* (CSIP) and it requires the constraints to be satisfied for an infinite number of admissible noise vectors $W \in \tilde{\mathbb{W}}^N$ and thus there are (potentially) *uncountably many* such constraints. We translated the problem (6) to the SIP (9) in order to establish a tractable algorithm that solves (6) in an *exact fashion* by means of the MSA algorithm (we refer to §A.2 and [DACC22] for more details on the algorithm).

We direct our attention to the SIP (9). To this end, define

$$(10) \quad \bar{N} := \dim(\theta) + \dim(\eta) + \dim(r),$$

$\widehat{N} := \overline{N} \cdot N$, and the function $\widetilde{\mathbb{W}}^{\widehat{N}} \ni \mathcal{W} := (W^1, \dots, W^{\overline{N}}) \mapsto \mathcal{G}(\mathcal{W}; \bar{x}) \in \mathbb{R}$ for each $\bar{x} \in X_N$ by

$$(11) \quad \mathcal{G}(\mathcal{W}; \bar{x}) := \inf_{\theta, \eta, r} \left\{ r \left| \begin{array}{l} \text{constraints in (9) for all} \\ W^i \in \widetilde{\mathbb{W}}^N, i \in [1; \overline{N}] \end{array} \right. \right\}.$$

Observe that the problem (11) is a *relaxed* version of the SIP (9), where all the constraints in (11) need to be satisfied for *finite* number of indices W^i for $i \in [1; \overline{N}]$; and the quantity \overline{N} has a precise characterization given in (10). This is in contrast to the case in (9), where all the constraints needed to be satisfied for *all* $W \in \widetilde{\mathbb{W}}^N$, i.e., for all $\bar{w}_t \in \widetilde{\mathbb{W}}$ for each $t \in [0; N-1]$. We shall refer to the problem (11) associated with the function $\mathcal{G}(\cdot; \bar{x})$, for each \bar{x} , as the *inner problem* in the sequel.

Finally, to extract the exact solution to the SIP (9) one needs to globally optimize $\mathcal{W} \mapsto \mathcal{G}(\mathcal{W}, \bar{x})$ over $\mathcal{W} \in \widetilde{\mathbb{W}}^{\widehat{N}}$. Precisely, consider the maximization problem

$$(12) \quad \sup_{\mathcal{W}} \{ \mathcal{G}(\mathcal{W}; \bar{x}) \mid \mathcal{W} \in \widetilde{\mathbb{W}}^{\widehat{N}} \},$$

which will be called the *outer problem* thereof, and this construct furnishes a single numerical method to solve (9) using the MSA algorithm described in [DACC22]. As emphasized earlier, our algorithm algorithm solves the SIP (9) *exactly* in the sense that the *optimal value* of the original SIP (9) and the global maximization problem (12) are the same (see Theorem 3.3).

3. Main results: Theory and Algorithms

In this section, we present our main theoretical results, with proofs available in Appendix B and Appendix C. First, we offer a high-level overview of our findings:

- (1) (§3.1) The primary object is the minmax robust MPC problem (2) which we, via several intermediate steps, converted into the SIP (9). Various system theoretic properties of (9) under the application of the MSA algorithm are recorded in §3.1 along with a global optimization algorithm to solve (12); see Algorithm 1 (SimAnnSIP). The primary result is Theorem 3.3; proof is given in Appendix B.
- (2) (§3.2, §3.3, §3.4, §3.5) We then leverage Algorithm 1 and establish two different feedback learning algorithms. For a given $\varepsilon > 0$, both the algorithms theoretically provide guarantees for uniform approximation of the unknown optimal policy $\mu_0^*(\cdot)$ via the approximate policy $\mu_0^\dagger(\cdot)$, under certain regularity assumptions on $\mu_0^*(\cdot)$.
 - (QuIFL) Algorithm 2: based on quasi-interpolation, for low-dimensional systems. The primary result is Theorem 3.8; proof is given in Appendix C.
 - (NNFL) Algorithm 3: based on neural networks, for moderate-dimensional systems. The primary result is Theorem 3.10; proof is given in Appendix C.

3.1. The application of the MSA to the minmax problem. We begin by recording one of our chief observations concerning the problems (6) and (9). Let us fix some notations. Let $\mathcal{X} := \mathbb{R}^{mN \times dN} \times \mathbb{R}^{mN} \times [0, +\infty[$; by $x_{\theta, \eta}(t; \bar{x}, W)$ we mean the solution to the recursion (3) at time t with initial state \bar{x} under the control (5) and disturbance sequence W . We will continue to denote the terminal state $x_{\theta, \eta}(N; \bar{x}, W)$ by x_N in the sequel.

Lemma 3.1. *Consider the OCP (6) and the SIP (9) with their associated data and notations. Define the set of admissible (θ, η, r) by*

$$\mathcal{S} := \{(\theta, \eta, r) \in \mathcal{X} \mid \text{the constraints of the SIP (9) hold}\}.$$

Then \mathcal{S} is closed and convex.

The next assumption is a technical requirement which states that (6) is strictly feasible for $W^i \in \tilde{\mathbb{W}}^N$ for each $i = 1, \dots, \bar{N}$. This in turn implies strict feasibility of the optimization problem (9), and consequently, that of the relaxed problem (11).

ASSUMPTION 3.2. We stipulate for the OCP (6) that the following Slater-type condition holds: there exists a nonempty open set $O \subset \text{int } \mathbb{M} \times \text{int } \mathbb{U}$ such that

$$\bigcap_{(W^i)_{i=1}^{\bar{N}}} \left\{ (\theta, \eta, r) \left| \begin{array}{l} \mathbb{J}_N(\bar{x}, \theta^i, \eta^i, W^i) - r < 0, x_0 = \bar{x}, x_N \in \text{int } \mathbb{M}_F, \\ (x_{\theta, \eta}^i(t; \bar{x}, W^i), u_t^i + v_t^i) \in O, W^i \in \tilde{\mathbb{W}}^N \end{array} \right. \right\}$$

is nonempty.

Theorem 3.3. Consider the OCP (6) and the corresponding SIP (9) together with their associated data and notations, and let the Assumption 3.2 hold. Fix $\bar{x} \in X_N$ and consider the global maximization problem (12). Then:

(3.3-a) $\tilde{\mathbb{W}}^{\bar{N}} \ni \mathcal{W} \mapsto \mathcal{G}(\mathcal{W}; \bar{x}) \in \mathbb{R}$ is upper semicontinuous for every $\bar{x} \in X_N$,

(3.3-b) there exists an \bar{N} -tuple \mathcal{W}^* that solves (12), and

(3.3-c) $\mathbb{J}_N^*(\bar{x}) = \mathcal{G}(\mathcal{W}^*; \bar{x})$ for all $\bar{x} \in X_N$.

REMARK 3.4. Theorem 3.3 asserts that it is sufficient to consider only \bar{N} -many disturbance realizations W^i for $i \in \{1, \dots, \bar{N}\}$ for which the constraints of the problem (11) need to be satisfied; then the resulting relaxed problem solves the original SIP (9). To obtain such an \bar{N} -tuple optimal point \mathcal{W}^* , the maximization problem (12) in Theorem 3.3 must be solved globally on $\tilde{\mathbb{W}}^{\bar{N}}$, and at the optimal point \mathcal{W}^* the value of the minmax problem (6) and (12) are identical.

A global optimization based algorithm to solve (6): Algorithm 1 systematically addresses the global maximization problem (12) arising from numerically solving (9). While any suitable global optimizer can be used, we employ simulated annealing for its scalability with dimensionality but do not recommend it universally.

Algorithm 1: (SimAnnSIP) Global optimization algorithm to solve (12)

Data : Stopping criterion $SC(\cdot)$, threshold for the stopping criterion τ , fix $\bar{x} \in X_N$.

Initialize: initialize the constraint indices $(W_{\text{init}}^1, W_{\text{init}}^2, \dots, W_{\text{init}}^{\bar{N}}) \in \tilde{\mathbb{W}}^{\bar{N}}$, initial guess for \mathcal{G}_{max} , initial guess for the solution $\bar{\theta}$ and $\bar{\eta}$

- 1 **while** $SC(n) \leq \tau$ **do**
- 2 Sample (via simulated-annealing) the disturbance constraint set $\mathcal{W}^n := (W^{n,1}, W^{n,2}, \dots, W^{n,\bar{N}}) \in \tilde{\mathbb{W}}^{\bar{N}}$
- 3 Solve the *inner-problem* and evaluate $\mathcal{G}_n = \mathcal{G}(\mathcal{W}^n; \bar{x})$ as defined in (11)
- 4 Recover the solution $\theta_n, \eta_n, r_n \in \arg \min_{(\bar{\theta}, \bar{\eta}, \bar{r})} \{\bar{r} \mid \text{constraints in (11) hold at } \mathcal{W}^n\}$
- 5 **if** $\mathcal{G}_n \geq \mathcal{G}_{\text{max}}$ **then**
- 6 Set $\mathcal{G}_{\text{max}} \leftarrow \mathcal{G}_n, \bar{\theta} \leftarrow \theta_n, \bar{\eta} \leftarrow \eta_n$
- 7 Update $n \leftarrow n + 1$
- 8 **end**
- 9 **end**

3.2. QuIFL: feedback learning for low-dimensional systems. We present an algorithm to learn an approximate policy $\mu_0^\dagger(\cdot)$, offline, for low-dimensional systems, which, by design, satisfies the approximation bound $\|\mu_0^*(\cdot) - \mu_0^\dagger(\cdot)\|_{\text{u}} \leq \varepsilon$, for any preassigned $\varepsilon > 0$. Our approximation scheme relies on the following assumption regarding the regularity of $\mu_0^*(\cdot)$.

ASSUMPTION 3.5. We assume that the policy $\bar{x} \mapsto \mu_0^*(\bar{x})$ is Lipschitz continuous with rank L_0 .

Algorithmic steps to generate $\mu_0^\dagger(\cdot)$ via QuIFL: We employ Algorithm 1 to generate the approximation-aware policy $\mu_0^*(\cdot)$ at grid points of a uniform grid on the state-space \mathbb{M} . Armed with this (state, action) data $(mh, \mu_0^*(mh))$ where $mh \in \mathbb{M} \cap \{mh \mid m \in \mathbb{Z}^d, h > 0\}$, before proceeding to learn $\mu_0^\dagger(\cdot)$, we perform an extension procedure on the domain of $\mu_0^*(\cdot)$.⁵ Moreover, we require the extended policy to maintain Lipschitz continuity.

To this end, let $\widehat{X}_N := X_N \cap \{mh \mid m \in \mathbb{Z}^d\}$ be an h -net [HPM06] of X_N ; define the (component-wise) extended policy by

$$(13) \quad \mathbb{R}^d \ni x \mapsto \mu_E^*(x) := \inf_{y \in \widehat{X}_N} (\mu_0^*(y) + L_0 \|x - y\|_2).$$

It is easy to check that $\mu_E^*(\cdot)$ is Lipschitz on \mathbb{R}^d with the same rank L_0 ; see [Loj88, Appendix 3, Lemma 1]. In the sequel, we shall overload notation and continue to label the policy $\mu_E^*(\cdot)$ after extension to \mathbb{R}^d as $\mu_0^*(\cdot)$ itself.

We are now ready to apply our first approximation scheme, based on quasi-interpolation, to learn $\mu_0^\dagger(\cdot)$.⁶ For the extended policy $\mu_0^*(\cdot)$ the quasi-interpolation scheme is given by

$$(14) \quad \widehat{\mu}_0(x) := \mathcal{D}^{-d/2} \sum_{m \in \mathbb{Z}^d} \mu_0^*(mh) \psi\left(\frac{x - mh}{h\sqrt{\mathcal{D}}}\right)$$

for all $x \in \mathbb{R}^d$; where $\psi(\cdot)$ is a continuous generating/basis function that needs to satisfy

- *the continuous moment condition of order $M \in \mathbb{N}^*$* , i.e.,

$$(15) \quad \int_{\mathbb{R}^d} \psi(y) dy = 1 \text{ and } \int_{\mathbb{R}^d} y^\alpha \psi(y) dy = 0 \\ \text{for all } \alpha, 1 \leq [\alpha] < M;$$

where $\alpha \in \mathbb{N}^d$ is a multi-index and $[\alpha] = \alpha_1 + \dots + \alpha_d$.

- *the decay condition:* For all $\alpha \in \mathbb{N}^d$ satisfying $0 \leq [\alpha] \leq \lfloor d/2 \rfloor + 1$, the function $\psi(\cdot)$ is said to satisfy the decay condition of exponent K if there exist $C_0 > 0$ and $K > d$ such that

$$(16) \quad (1 + \|x\|)^K |\partial^\alpha \psi(x)| \leq C_0 \quad \text{for } x \in \mathbb{R}^d.$$

Then from [MS07, Theorem 2.25] or [GC25, Theorem III.1] we have the estimate

$$(17) \quad \|\widehat{\mu}_0(\cdot) - \mu_0^*(\cdot)\|_{\text{u}} \leq C_\gamma L_0 h \sqrt{\mathcal{D}} + \Delta_0(\psi, \mathcal{D}) \text{ on } \mathbb{R}^d,$$

where $\Delta_0(\psi, \mathcal{D}) := \mathcal{E}_0(\psi, \mathcal{D}) \|\mu_0^*(\cdot)\|_{\text{u}}$ is the saturation error, $C_\gamma := M \cdot \Gamma(M)/\Gamma(M+2)$ is a constant (where Γ denotes the standard Gamma function), and the term $\mathcal{E}_0(\psi, \mathcal{D})$ is

$$(18) \quad \mathcal{E}_0(\psi, \mathcal{D})(\cdot) := \sup_{x \in \mathbb{R}^d} \sum_{\nu \in \mathbb{Z}^d \setminus \{0\}} \mathcal{F}\psi(\sqrt{\mathcal{D}}\nu) e^{2\pi i \langle x, \nu \rangle}.$$

⁵The extension is essential. Indeed, by design, $\mu_0^*(\cdot)$ is defined on X_N ; but to prove Theorem 3.8 ahead the domain of $\mu_0^*(\cdot)$ must be extended to \mathbb{R}^d . This is a technical requirement.

⁶For a brief background on the quasi-interpolation scheme we refer to [GC25, §III].

Note that, for each $x \in \mathbb{R}^d$, (14) constitute a summation over the lattice \mathbb{Z}^d . Instead, we use the finite-sum truncated approximant to learn our approximate policy. Define $\mathbb{F}_x(\rho) := \{mh \mid mh \in \mathbb{Z}^d\} \cap B_2^d[x, \rho h]$ and consider the sum

$$(19) \quad \mu_0^*(x) := \mathcal{D}^{-d/2} \sum_{mh \in \mathbb{F}_x(\rho)} \mu_0^*(mh) \psi \left(\frac{x - mh}{h\sqrt{\mathcal{D}}} \right)$$

for all $x \in \mathbb{R}^d$. Note that for any given $\bar{\varepsilon} > 0$, by appropriately choosing ρ , the difference between $\mu_0^*(\cdot)$ and $\mu_0^\dagger(\cdot)$ can be uniformly bounded by $\bar{\varepsilon}$ for all $x \in \mathbb{R}^d$. Hence, the use of $\mu_0^\dagger(\cdot)$ is justified; see [MS07, §2.3.3] for more details.

Thus, three quantities in (19) — ρ , h , and \mathcal{D} — can be picked **depending on the prescribed error margin** to ensure that the total **uniform** error, stays within the preassigned bound ε . The formal selection process for the tuple $(h, \mathcal{D}, \rho) \in]0, +\infty[^3$ is outlined in Theorem 3.8 and Algorithm 2.

3.3. Approximation and stability guarantees under QuIFL.

ASSUMPTION 3.6. The following standard assumptions [MF19] must be satisfied for recursive feasibility of the problem (6) and closed-loop stability of (3) under the policy $\mu_0^*(\cdot)$:

- There exists a continuous map $\mathbb{M}_F \ni x \mapsto \mu_F(x) \in \mathbb{U}$ such that $c_F(Ax + B\mu_F(x)) - c_F(x) \leq -c(x, \mu_F(x))$ and $Ax + B\mu_F(x) + \tilde{w} \in \mathbb{M}_F$ for every $(x, \tilde{w}) \in \mathbb{M}_F \times \tilde{\mathbb{W}}$.
- There exists $\rho_1(\cdot) \in \mathcal{K}$ such that for every $x \in \mathbb{M}_F$ and for every $\tilde{w} \in \tilde{\mathbb{W}}$, $c_F(\cdot)$ satisfies $c_F(Ax + B\mu_F(x) + \tilde{w}) - c_F(x) \leq -c(x, \mu_F(x)) + \rho_1(\|\tilde{w}\|_\infty)$.⁷

REMARK 3.7. Given Assumptions 2.2 and 3.6, it follows from [MF19, §3] that the problem (6) remains recursively feasible. Furthermore, when $\mu_0^*(\cdot)$ is applied, the value function $\mathbb{J}_N^*(\cdot)$ exhibits a *descent behavior*

$$(20) \quad \mathbb{J}_N^*(x^+) - \mathbb{J}_N^*(x) \leq -c(x, \mu_0^*(x)) + \rho_1(W_{\sup}).$$

for all $x \in X_N$ and $\tilde{w} \in \tilde{\mathbb{W}}$, where the successor state is defined as $x^+ := Ax + B\mu_0^*(x) + \tilde{w}$, and the term W_{\sup} represents the supremum of the disturbance magnitudes, i.e., $W_{\sup} := \sup\{|\tilde{w}| \mid \tilde{w} \in \tilde{\mathbb{W}}\}$.

Against this backdrop, here is our second technical result concerning the approximate feedback policy $\mu_0^\dagger(\cdot)$ learned by QuIFL (proof given in Appendix C):

Theorem 3.8. Consider the OCP (6) along with its associated data. Let $\mu_0^*(\cdot)$ be the corresponding approximation-aware MPC policy and suppose that assumptions 2.2 and 3.5 hold. Then:

(3.8-a) For every given $\varepsilon > 0$, there exist a generating function $\psi(\cdot) \in \mathcal{S}(\mathbb{R}^d)$, a triple $(h, \mathcal{D}, \rho) \in]0, +\infty[^3$, such that the approximate feedback map $X_N \ni x \mapsto \mu_0^\dagger(x) \in \mathbb{U}$ defined in (19) is within a uniform error margin ε from $\mu_0^*(\cdot)$; to wit,

$$\|\mu_0^*(x) - \mu_0^\dagger(x)\| \leq \varepsilon \quad \text{for all } x \in X_N.$$

(3.8-b) Suppose that Assumption 3.6 holds and given the initial state x , let x^+ be the state at the next time instant. Then under $X_N \ni x \mapsto \mu_0^\dagger(x)$ learned via Algorithm 2: QuIFL, the closed-loop process $x^+ = Ax + B\mu_0^\dagger(x) + w$ corresponding to the system (1) is ISS-like stable in the sense of Definition A.2.

⁷Definition of class \mathcal{K} , \mathcal{K}_∞ , and \mathcal{KL} functions can be found in [Kha02, Chapter 4, Definition 4.2].

Algorithm 2: QuIFL: Quasi-interpolation-driven feedback synthesis

Data : $\mu_0^*(\cdot)$ on \widehat{X}_N
Initialize : Lipschitz constant L_0 of the policy $\mu_0^*(\cdot)$
Extend : Extend $\mu_0^*(\cdot)$ to \mathbb{R}^d using (13)
Learning: \circ Fix $\varepsilon > 0$ and choose the tuple $(\psi(\cdot), h, \mathcal{D}, \rho) \in \mathcal{S}(\mathbb{R}^d) \times]0, +\infty[^3$;
 \circ Compute $\mu_0^\dagger(\cdot)$ via (19) and restrict $\mu_0^\dagger(\cdot)$ to X_N .

REMARK 3.9. Algorithm 2 represents a significant advancement over [GC25], as it satisfies all the properties **(T-a)**–**(T-c)** outlined in contribution (see §1). It introduces a novel semi-infinite optimization-driven approach — both theoretical and algorithmic — for solving the minmax MPC problem *exactly* while integrating it with a quasi-interpolation-based oracle for low-dimensional systems. In contrast, [GC25] relied on off-the-shelf solvers for minmax optimization problems without contributing new methodological developments in this area.

3.4. NNFL: feedback learning for moderate-dimensional systems. Due to the use of a uniform grid, the synthesis approach established in §3.2–§3.3 is suitable for learning approximate policies only if the underlying dynamical system is of low dimension. To address this, particularly for moderate-dimensional systems, we develop an alternative approach using deep neural networks with ReLU activation functions. By leveraging recent results on uniform approximation using ReLU networks [SYZ22], we provide guarantees for *uniform* approximation error associated with the learning process, along with closed-loop stability guarantees, similar to Theorem 3.8. See Theorem 3.10 ahead in §3.5.

Algorithmic steps to generate $\mu_0^\dagger(\cdot)$ via NNFL: Recall that $\mu_0^*(\cdot)$ is the approximation-aware policy generated via Algorithm 1. For learning the a feedback we will employ a feedforward ReLU neural network architecture [DHP21] and we denote the approximate policy to $\mu_0^*(\cdot)$ generated via the ReLU network by

$$(21) \quad \mu_0^\dagger(\cdot) := \Upsilon_{\mu_0^*(\cdot)}^{W,L}(\text{ReLU}(\cdot); d, d'),$$

where for fixed W (width), L (depth), d (input dimension), d' (output dimension), and with $x \mapsto \text{ReLU}(x) := \max\{0, x\}$ (activation function), the function $\Upsilon_{\mu_0^*(\cdot)}^{W,L}(\text{ReLU}(\cdot); d, d')$ denotes the ReLU approximation of the policy $\mu_0^*(\cdot)$. The (state, action) data for training the ReLU network is generated by sampling initial states \bar{x} from the set \mathbb{M} and solving (6) using the global optimization problem (12) via Algorithm 1. We denote by \mathcal{X}_0 the set of sampled initial states, obtained either through structured *grid-based* sampling or *uniform random* sampling over the domain \mathbb{M} . While a grid-based sampling is necessary for the quasi-interpolation-based construction of the approximate policy $\mu_0^\dagger(\cdot)$ described in §3.2, neural network approximation does not impose such restrictions, making the algorithm potentially scalable to systems with moderately many dimensions.

Recall Corollary A.5 in Appendix A.3. In our context, we replace $f(\cdot)$ and $f_{\text{ReLU}}(\cdot)$ in Corollary A.5 with $\mu_0^*(\cdot)$ and its ReLU-approximant $\mu_0^\dagger(\cdot)$, respectively, and the estimate (37) can be rewritten as:

$$(22) \quad \|\mu_0^*(\cdot) - \mu_0^\dagger(\cdot)\|_{\text{u}} \leq 131\sqrt{d}L_0 \left(\left(\frac{W}{3^{d+5}d} \right)^2 \left(\frac{L-18-2d}{22} \right)^2 \log_3 \left(\frac{W}{3^{d+5}d} + 2 \right) \right)^{-1/d},$$

where L_0 is the Lipschitz rank of the feedback policy $\mu_0^*(\cdot)$ and W, L are the *width* and *depth* of the network respectively. The values of W and L are to be selected **according to the prescribed error margin**. To this end, we fix an error margin $\varepsilon > 0$, and proceed with the aforementioned selection as follows:

- ▷ We may begin by either setting a value to the network's width W or depth L . The reasons influencing this choice include the facts that a greater width increases the number of trainable parameters, thus requiring a larger number of data points, but a greater depth increases training complexity owing to higher-order nonlinearities.
- ▷ In accordance with the choice made in the previous step, if the value of the width W is set first, then the value for the depth L can be calculated using (22). Similarly, if the depth L is set first, then the width W found using the estimate (22). These estimates will be discussed in detail in §3.5.

The above procedure ensures that the error between $\mu_0^*(\cdot)$ and $\mu_0^\dagger(\cdot)$ stays uniformly within the prescribed bound ε . The complete process is given in Algorithm 3.

Algorithm 3: NNFL: Neural Network-driven feedback synthesis

Data : $\mu_0^*(\cdot)$ at points obtained from Algorithm 1

Initialize : Lipschitz rank L_0 of the policy $\mu_0^*(\cdot)$

Learning:

- Fix $\varepsilon > 0$ followed by setting a value for either *depth* L or the *depth* W for the ReLU network;
- For a fixed width, using (3.10-a), or for a fixed depth, using (3.10-b), estimate the depth or the width depending on the fixed ε ;
- Generate the training dataset using Algorithm 1 on a set of initial states \mathcal{X}_0 , sampled from \mathbb{M} .
- Tune hyperparameters and train the NN to generate $\mu_0^\dagger(\cdot)$ such that $\|\mu_0^*(x) - \mu_0^\dagger(x)\| \leq \varepsilon$ for all $x \in \mathbb{M}$.

3.5. Approximation and stability guarantees under NNFL. Here is our key result on ReLU neural network approximation (proof given in Appendix C):

Theorem 3.10. *Consider the constrained OCP (6) along with its associated data. Let $\mu_0^*(\cdot)$ be the corresponding approximation-aware MPC policy and suppose that assumptions 2.2 and 3.5 hold. Then:*

(3.10-a) *For every given $\varepsilon > 0$ and a fixed width $\mathcal{W}_0 \geq 3^{d+4}d$, there exists $L \in \mathbb{N}^*$, and an approximate feedback map $X_N \ni x \mapsto \mu_0^\dagger(x) \in \mathbb{U}$ realized by a ReLU neural network of width \mathcal{W}_0 and depth L such that the uniform error estimate*

$$\|\mu_0^*(x) - \mu_0^\dagger(x)\| \leq \varepsilon \quad \text{holds for all } x \in X_N.$$

(3.10-b) *For every given $\varepsilon > 0$ and a fixed depth $\mathcal{L}_0 \geq 29 + 2d$, there exists $W \in \mathbb{N}^*$, and an approximate feedback map $X_N \ni x \mapsto \mu_0^\dagger(x) \in \mathbb{U}$ realized by a ReLU neural network of depth \mathcal{L}_0 and width W such that the uniform error estimate*

$$\|\mu_0^*(x) - \mu_0^\dagger(x)\| \leq \varepsilon \quad \text{holds for all } x \in X_N.$$

(3.10-c) *Suppose that Assumption 3.6 holds and given the initial state x let x^+ be the state at the next time instant. Then under $X_N \ni x \mapsto \mu_0^\dagger(x)$ constructed via Algorithm 3: NNFL, the closed-loop process $x^+ = Ax + B\mu_0^\dagger(x) + w$ corresponding to the system (1) is ISS-like stable in the sense of Definition A.2.*

REMARK 3.11. In practice, the width and depth of ReLU networks required by Theorem 3.10 are often significantly larger than what is empirically necessary. This discrepancy stems from the fact that the bounds in [SYZ22] were derived for Lipschitz continuous functions, which can result in overly conservative estimates. Our numerical experiments

demonstrate that much shallower networks are often sufficient to achieve accurate approximations, indicating that the theoretical requirements may not always align with practical realities. Moreover, the non-exactness inherent in typical training procedures underscores the importance of a post-hoc validation of the approximated feedback map to ensure its reliability and effectiveness, thereby providing practical guarantees for the approximation.

4. Numerical experiments

In this section, we focus on two examples to illustrate the numerical fidelity of the three main algorithms established in the preceding sections. The first example is the more comprehensive one — it considers a minmax OCP for a second-order system, allowing clear visualization of the feedback maps learned by Algorithms 2 and 3. Additionally, by demonstrating a larger feasibility region, this example highlights why Algorithm 1 outperforms standard scenario-driven robust optimization methods. For the fourth-order example, we use only Algorithm 3 to construct the state and control trajectories. For both problems, we employed Algorithm 1 via solving the *inner problem* using MOSEK [ApS19] in conjunction with YALMIP [Lof04] in MATLAB and for the *outer problem*, which is a global maximization, we employed simulated annealing. For the simulated annealing, we used MATLAB's global optimization toolbox; we kept the initial temperature 10, and the number of iterations 1500 with the exponential temperature decay of the form $T_t = 0.99T_{t-1}$, where T_t is the annealing temperature at the t^{th} iteration. We performed our numerical computations related to data generation on MATLAB 2019b using the parallel computation toolbox in an 36 core server with Intel(R) Xeon(R) CPU E5 – 2699 v3, 4.30 GHz with 128 Gigabyte of RAM.

EXAMPLE 4.1. Consider the dynamical system [GC12, GC24]:

$$(23) \quad x_{t+1} = \begin{pmatrix} 0.732 & -0.086 \\ 0.172 & 0.990 \end{pmatrix} x_t + \begin{pmatrix} 0.060 \\ 0.006 \end{pmatrix} u_t + \begin{pmatrix} 0.3 & 0.4 \\ 0.2 & 0.15 \end{pmatrix} w_t.$$

Fix $N = 5$, and define the discrete-time OCP

$$(24) \quad \begin{aligned} & \inf_{\pi(\cdot)} \sup_w \quad \langle x_N, Px_N \rangle + \sum_{t=0}^{N-1} \langle x_t, Qx_t \rangle + \langle u_t, Ru_t \rangle \\ & \text{subject to} \quad \begin{cases} (23), x_0 = \bar{x}, x_t \in \mathbb{M}, \text{ and } u_t \in \mathbb{U} \\ \text{for all } (t, w) \in [0; N-1] \times \mathbb{W}^N, \end{cases} \end{aligned}$$

where $\mathbb{M} := \{x = (x_1, x_2) \in \mathbb{R}^2 \mid \|x\|_\infty \leq 1.5\}$, $\mathbb{U} := \{u \in \mathbb{R} \mid |u| \leq 2\}$, and $\mathbb{W} := \{w \in \mathbb{R} \mid \|w\|_\infty \leq 0.05\}$. The state weighting matrix $Q := I_{2 \times 2}$ the 2×2 -identity matrix, the control weighting matrix $R := 0.01$, and $P := \begin{pmatrix} 5.5461 & 4.9873 \\ 4.9873 & 10.4940 \end{pmatrix}$. We fixed $\varepsilon = 0.03$, which is a uniform approximation error margin. According to our formulation (6) we defined the set $\tilde{\mathbb{W}} := [-0.05, 0.05] \oplus B[-0.03, 0.03]$ and $\tilde{w}_t = w_t + Bv_t$ takes values in $\tilde{\mathbb{W}}$. Recall that $W := (\tilde{w}_0, \dots, \tilde{w}_{N-1})$; next we employed the parameterization (5), and arrived at the approximation-aware OCP

$$(25) \quad \begin{aligned} & \min_{(\theta, \eta)} \max_W \quad \langle x_N, Px_N \rangle + \sum_{t=0}^{N-1} \langle x_t, Qx_t \rangle + \langle u_t, Ru_t \rangle \\ & \text{subject to} \quad \begin{cases} x_{t+1} = Ax_t + Bu_t + Bv_t + w_t, \\ x_0 = \bar{x}, x_t \in \mathbb{M}, \text{ and } u_t + \zeta_t \in \mathbb{U} \\ \text{for all } (t, W) \in [0; N-1] \times \tilde{\mathbb{W}}^N. \end{cases} \end{aligned}$$

Data generation via Algorithm 1: We translated (25) as a CSIP of the form 9, where the constraints are needed to be satisfied for an infinite number disturbance realizations \tilde{w}_t for

each $t = 0, \dots, N - 1$. But Algorithm 1 indicates that we need only \bar{N} -many constraints to be encoded in the algorithm, and for the problem (25), $\bar{N} = \dim(\theta) + \dim(\eta) + \dim(r) = 50 + 5 + 1 = 56$.

Next, the state-space $[-1.5, 1.5] \times [-1.5, 1.5]$ was equipped with a uniform cardinal grid corresponding to $h = 0.02$ leading to 22801 points and at each of these points we solved the SIPs independently (offline) via Algorithm 1 to generate the (state, action) data. The preceding choice of h is *not* arbitrary and will become evident shortly, in particular this choice of h depends on the error-margin ε . The convergence of the simulated annealing associated with the outer problem can be verified from the rightmost subfigure of Figure 2, where we see that the algorithm almost converges after 10^3 iterations, and the variations between multiple runs of the simulated annealing are insignificant.

Before moving to the learning procedure via Algorithm (2) and Algorithm (3), we compared the region of attraction (i.e., the feasible region X_N for (25)) of the feedback $\mu_0^*(\cdot)$ obtained by using Algorithm 1 with the robust optimization module in YALMIP, creating a uniform grid of step size $h = 0.02$. Observe that:

- (1) The feasible region X_N obtained by using Algorithm 1 is substantially larger than the one obtained from YALMIP's robust optimization module [Löf12]; see the leftmost subfigure of Figure 2. This is a desirable feature of any MPC algorithm; a bigger region of attraction implies the feasibility of the problem for a larger number of points. In particular, solving the problem (25) on a uniform grid with step size $h = 0.02$, Algorithm 1 produced 700 infeasible points, while the method in [Löf12] yielded 1436 points. This represents a 51.25% reduction in infeasible points with Algorithm 1.
- (2) The state trajectories obtained by employing Algorithm 1 and YALMIP's robust optimization module with the region of attraction corresponding to Algorithm 1 in the background, follow almost the same path and converge to a set containing the origin $0 \in X_N \subset [-1.5, 1.5] \times [-1.5, 1.5]$; see right-hand subfigure in Figure 2.
- (3) The optimal value obtained from Algorithm 1 consistently exceeded that of the algorithm in [Löf04]; see Table 1. This is because Algorithm 1 provides exact solutions, closely tracking the original optimal value.

Table 1. Comparison of optimal values obtained by Algorithm 1 and the algorithm in [Löf12].

\bar{x}	Value (Alg. 1)	Value (Alg. [Löf12])
$(0.5, 0.5)^\top$	2.198	2.14
$(-1, 0.4)^\top$	1.794	1.489
$(1, -0.9)^\top$	2.623	2.25
$(-0.3, -0.7)^\top$	2.48	2.412

Learning via Algorithm 2: For the quasi-interpolation scheme, we employ the Laguerre-Gaussian basis function

$$(26) \quad x \mapsto \psi(x) := \frac{1}{\pi} \left(3 - 3\|x\|^2 + \frac{1}{2}\|x\|^4 \right) e^{-\|x\|^2},$$

that belongs to $\mathcal{S}(\mathbb{R}^2)$ and satisfies the moment condition of order $M = 6$, which means that the constant $C_\gamma = 1/7$. Recall that we fixed the error margin $\varepsilon = 0.03$, i.e., we want $\|v_t\|_\infty \leq 0.03$. Next, fixing the shape parameter $\mathcal{D} = 2$, we obtain the value of $h = \frac{\varepsilon}{3C_\gamma L_0 \sqrt{\mathcal{D}}} \approx 0.02$, where we have employed a rough, and conservative estimate of the Lipschitz constant $L_0 = 2.5$ of $\mu_0^*(\cdot)$. We picked $\rho = 4$. With these ingredients,

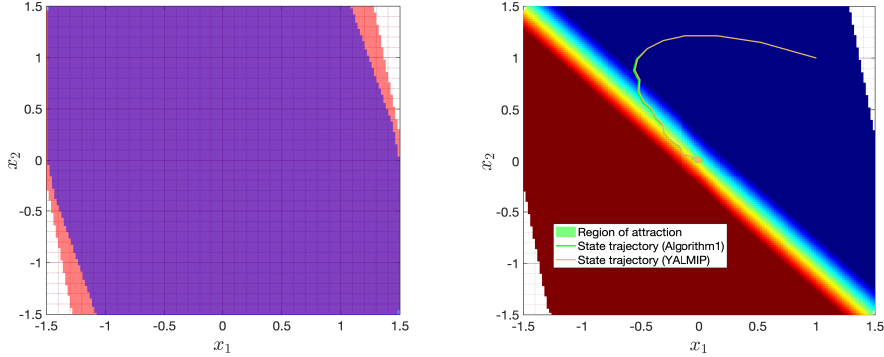


Figure 2. The superimposed regions of attraction — computed using YALMIP (violet) and Algorithm 1 (magenta) — are shown in the left-hand subfigure. The right-hand subfigure displays sample phase-space trajectories starting from the initial state $\bar{x} := (1 \ 1)^\top$, obtained using both Algorithm 1 and YALMIP’s robust optimization module.

after performing the extension procedure (13), for all $x \in \mathbb{R}^2$, we employed the quasi-interpolation formula

$$(27) \quad \mu_0^\dagger(x) := \frac{1}{\pi \mathcal{D}} \sum_{mh \in \mathbb{F}_x(\rho)} \mu_0^*(mh) \left(3 - \frac{3\|x - mh\|^2}{h^2 \mathcal{D}} + \frac{2\|x - mh\|^4}{h^4 \mathcal{D}^2} \right) e^{-\frac{\|x - mh\|^2}{\mathcal{D}h^2}}$$

for the approximate feedback learning. The policies $\mu_0^\dagger(\cdot)$ and $\mu_0^*(\cdot)$ can be seen in Figure 3 (the left-hand most and the right-hand subfigures, respectively), and the error surface is depicted in Figure 4 (the right-hand subfigure), from where it is evident that the error tolerance margin is strictly satisfied.

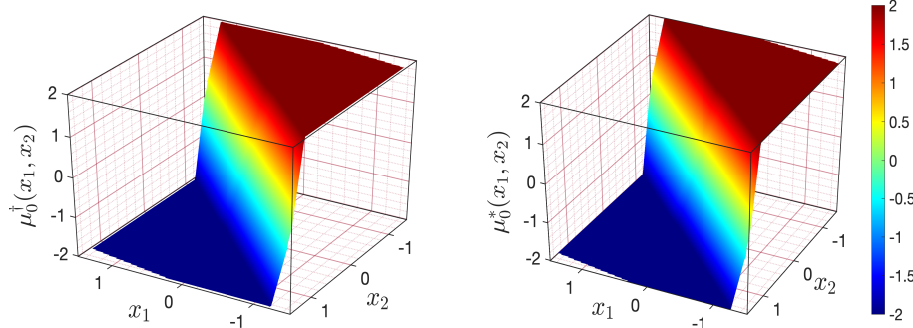


Figure 3. The left-hand and the right-hand subfigures depicts the learned policy $\mu_0^\dagger(\cdot)$ computed via Algorithm 2 and the policy $\mu_0^*(\cdot)$, respectively.

Learning via Algorithm 3: We move to the implementation details of the learning Algorithm 3 using the ReLU networks. We fixed $\varepsilon = 0.1$ and generated (state, action) data by solving the SIP via Algorithm 1, independently, in parallel, at each grid point of $[-1.5, 1.5] \times [-1.5, 1.5]$ with a step size of 0.01. The (state, action) data was used to train a ReLU neural network, excluding sampled initial states outside the feasible region. The final training dataset consisted of 87948 data points. Points for the testing set were sampled randomly from the feasible region amounting to a total of 10000 testing points. The neural network was trained using PyTorch on the NVIDIA Tesla P100 GPU. The input and output dimensions of the neural network were $d = 2$ and $d' = 1$. For illustration,

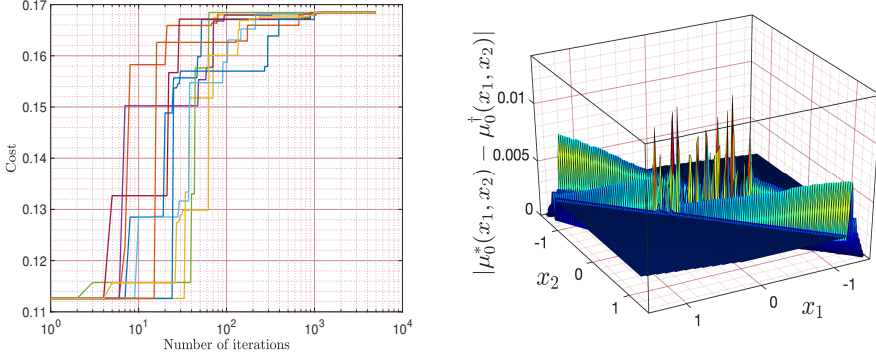


Figure 4. The left-hand subfigure shows that the optimal value consistently converges to the same value across multiple runs of simulated annealing when Algorithm 1 is employed. The right-hand subfigure depicts the error surface corresponding to the feedback policies in Figure 3; it can be seen that the prespecified error margin $\varepsilon = 0.03$ is respected

the width of the ReLU network W was fixed at 64, and using the estimates provided in (3.10-a), we obtained the value for the depth $L = \lceil 22\tilde{L} + 22 \rceil = 8721411$, where \tilde{L} is as given in (47). Training such a large network is computationally challenging, but a network with a much lower depth of $L = 4$ allows us to achieve our target error margin (verified empirically below). With these new parameters, our ReLU-network approximation $\mu_0^\dagger(\cdot)$ (following our previous notation in (21)) is:

$$(28) \quad \mu_0^\dagger(\cdot) := \Upsilon_{\mu_0^*(\cdot)}^{64,4}(\text{ReLU}(\cdot); 2, 1).$$

The training was done using supervised learning on the training data generated for 30000 epochs over 8 hours with a Stochastic Gradient Descent optimizer. The learning rate was 5×10^{-4} for all the epochs. A typical evolution of the training loss versus the epochs is depicted in Figure 6. Post-training, we generated the approximate feedback map using the neural network, and the result is shown in the left-hand subfigure in Figure 5. The approximation error is shown in the right-hand subfigure in Figure 5, and we note that it strictly satisfies the prespecified error-margin ε .

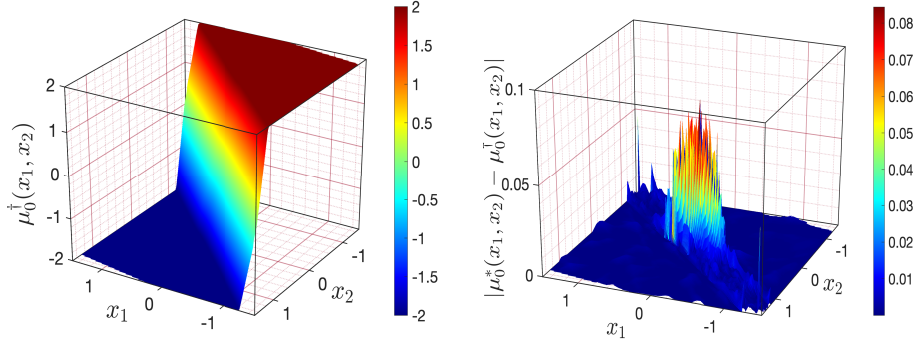


Figure 5. The approximate policy $\mu_0^\dagger(\cdot)$ (the left-hand subfigure) obtained via Algorithm 3 and the corresponding error surface (the right-hand subfigure).

Table 2 collects the computation-time data for the explicit feedback law $\mu_0^\dagger(\cdot)$ when Algorithm 2, Algorithm 3, and the algorithm established in [GC12] were employed, respectively. Both Algorithm 2 and Algorithm 3 were computationally faster compared to the

Table 2. Error margin and computation-time statistics. The algorithm in [GC12] is based on approximate multiparametric programming and there is no feature to control uniform approximation error. **CT.M.** ($\mu_0^\dagger(\bar{x})$) represents the per-point computation time to evaluate the learned feedback map in MATLAB.

Method	Uniform error	CT.M. ($\mu_0^\dagger(\bar{x})$) (in mil. sec.)
[GC12]	NA	15
Algorithm 2	$\varepsilon = 0.03$	0.2
Algorithm 3	$\varepsilon = 0.1$	1.6
RHC/MPC	NA	30

algorithm in [GC12]. For a fair comparison with the algorithm in [GC12], we employed MATLAB to check the online evaluation time of the policies $\mu_0^\dagger(\cdot)$ obtained via several algorithms listed in Table 2. However, we observed that, with Julia 10.5, the per-point computation time improved to 13.5 microseconds for Algorithm 2 and 0.01 microseconds for Algorithm 3. This demonstrates the advantage of data-driven approximation instead of multiparametric programming-based explicit methods. As discussed earlier, due to the

Table 3. Uniform and MSE error with varying depth and width of the network.

Depth	Width	MSE error	Uniform Error
4	64	9.620×10^{-6}	0.09
4	70	8.753×10^{-6}	0.09
4	75	1.020×10^{-5}	0.09
5	64	9.921×10^{-5}	0.09
6	64	1.109×10^{-6}	0.09
4	60	1.228×10^{-6}	0.10

large network dimension estimates, we trained smaller models and verified that they satisfy the prescribed bounds; see Table 3. We also performed a validation process.

Validation. For the post-hoc validation procedure we adopt the technique established in [HKTA18]. Let δ_h be the confidence parameter and $\tilde{\mu}$ be the empirical risk as defined in [HKTA18, §IV, B], then it was shown that with a confidence $1 - \delta_h$ the probability that the approximation error between the policies $\mu_0^\dagger(\cdot)$ and $\mu_0^*(\cdot)$ is below the prespecified tolerance $\varepsilon > 0$, along a trajectory with a random initial condition from X_N is larger than $\tilde{\mu} - \varepsilon_h$.⁸ The validation procedure is adapted to include external disturbance sequences W . For each initial point, multiple such disturbance sequences are rolled out and a constraint check is performed on all such sequences. We choose a $\delta_h = 0.01$ and $\mu_{\text{crit}} = 0.98$. For validation rollouts, we sample initial states uniformly from the feasible set X_N with the number of initial states $p = 50000$. The validation terminates with a $\tilde{\mu} = 0.9895$. Hence $\tilde{\mu} - \varepsilon_h > \mu_{\text{crit}}$ for the chosen parameters, validating the guarantees up to a confidence.

EXAMPLE 4.2. Consider the fourth-order system

$$(29) \quad x_{t+1} = Ax_t + Bu_t + Gw_t,$$

⁸See [HKTA18, Lemma 7, Equation 17] for more details on several quantities related to the probabilistic validation procedure.

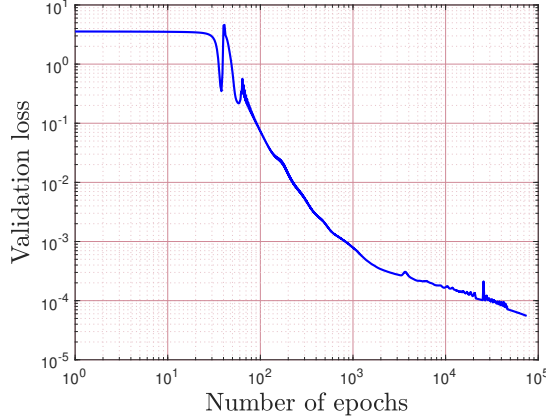


Figure 6. Validation loss of the NN during training.

with the state and the actuation matrices:

$$A := \begin{pmatrix} 0.40 & 0.37 & 0.29 & -0.72 \\ -0.21 & 0.64 & -0.67 & -0.04 \\ 0.83 & 0.01 & -0.28 & 0.38 \\ -0.07 & 0.60 & 0.55 & 0.49 \end{pmatrix}, B := \begin{pmatrix} 1.61 \\ 0.40 \\ -1.45 \\ -0.67 \end{pmatrix},$$

and $G := (1 \ 1 \ 1 \ 1)^\top$. Fix $N = 8$ and consider the OCP

$$(30) \quad \begin{aligned} & \min_{\pi(\cdot)} \max_w \sum_{t=0}^{N-1} \langle x_t, Qx_t \rangle + \langle u_t, Ru_t \rangle \\ & \text{subject to } \begin{cases} (29), x_0 = \bar{x}, x_t \in \mathbb{M}, \text{ and } u_t \in \mathbb{U} \\ \text{for all } (t, w) \in [0; N-1] \times \mathbb{W}^N, \end{cases} \end{aligned}$$

where $\mathbb{M} := \{x \in \mathbb{R}^4 \mid \|x\|_\infty \leq 5\}$, $\mathbb{U} := \{u \in \mathbb{R} \mid |u| \leq 0.2\}$, and $\mathbb{W} \in \mathbb{R} := \{w \mid \|w\|_\infty \leq 0.01\}$, with $Q := I_{4 \times 4}$ is a 4×4 -identity matrix, $R := 0.2$.

Approximation via the Algorithm 3: Fixing $\varepsilon = 0.1$, we solved the ensuing SIP arising from the problem (30) at 10^6 points which were independently and uniformly randomly sampled from the state space; the computer/server/solver specifications are identical to those in Example 4.1. Excluding the infeasible sample points, the final number of data points used for training were 735105. The input and output dimensions of the neural network were $d = 4$ and $d' = 1$. The width of the ReLU network W was fixed at 256, and using the estimates provided in (3.10-a), we obtained the value for the depth $L = \lceil 22\tilde{L} + 24 \rceil = 1735359$, where \tilde{L} is as given in 46. As in Example 4.1, training a network with much lower depth of $L = 6$ allowed us to achieve our error margin. With these parameters, our ReLU-network approximation $\mu_0^\dagger(\cdot)$ (following our previous notation in (21)) is:

$$(31) \quad \mu_0^\dagger(\cdot) := \Upsilon_{\mu_0^*(\cdot)}^{256,6}(\text{ReLU}(\cdot); 4, 1).$$

The training was done as in Example 4.1 using supervised learning on the training data generated for 4000 epochs with Stochastic Gradient Descent optimizer with a learning rate of 5×10^{-3} for around 12 hours of training time on the same setup. Post training validation uniform norm error of the approximated policy over the actual feedback was 0.0856, i.e., $\|\mu_0^\dagger(\cdot) - \mu_0^*(\cdot)\|_u \approx 0.0856$. Table 4 collects the computation-time and storage requirement data concerning the explicit feedback law $\mu_0^\dagger(\cdot)$ when Algorithm 3 and the Algorithm established in [GC12] (via YALMIP) was employed respectively. Same as

Table 4. Error margin and computation-time statistics where **CT.M.** ($\mu_0^\dagger(\bar{x})$) (in mil. sec.) represents the per-point computation time of the learned feedback map in MATLAB.

Method	Uniform error	CT.M. ($\mu_0^\dagger(\bar{x})$) (in mil. sec.)
[GC12]	NA	43
Algorithm 3	$\varepsilon = 0.1$	2.4
RHC/MPC	NA	270

Example 4.1, we observed that, with Julia 10.5, the per-point computation time improved to 3 microseconds for Algorithm 3. Figure 7 and 8 depict the performance of the

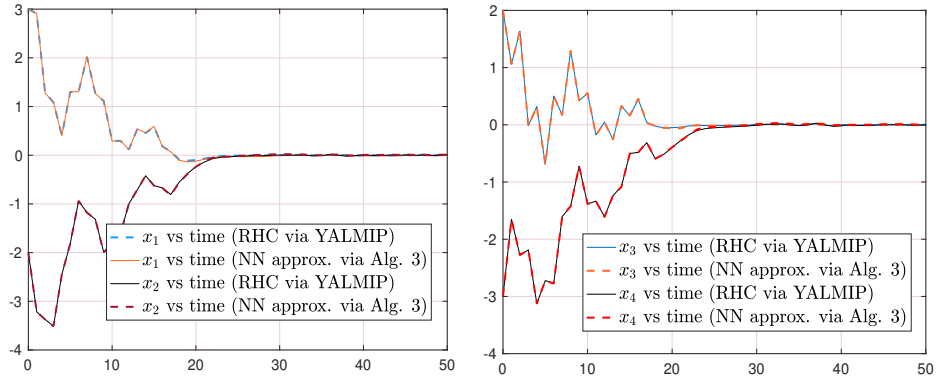


Figure 7. Evolution of the state trajectories starting from $\bar{x} = (3, -2, 2, -3)^\top$, generated using the explicit control law and the MPC/RHC control law; see Figure 8.

explicit control law generated by employing Algorithm 3 the corresponding closed-loop state trajectories. It can be seen that the states and the control satisfy the constraints and their trajectories almost overlap with the online receding horizon control and state trajectories with an improved computation time.

Validation. To adopt the same post-hoc validation technique as before. We choose a $\delta_h = 0.01$ and $\mu_{\text{crit}} = 0.99$. For validation rollouts, we sample initial states uniformly from the feasible set X_N with the number of initial states $p = 50000$. The procedure terminates

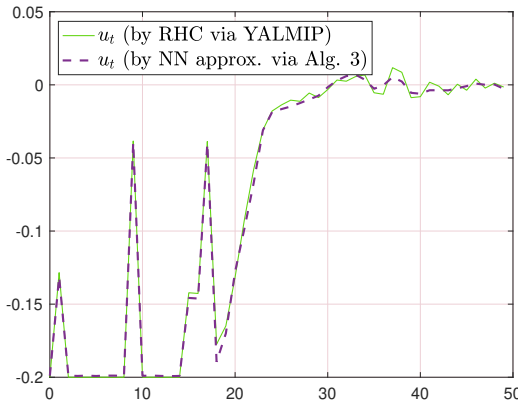


Figure 8. The explicit control law and the RHC law.

with a $\tilde{\mu} = 0.9935$, satisfying $\tilde{\mu} - \varepsilon_h > \mu_{\text{crit}}$ for the chosen parameters, validating the guarantees for the approximate explicit feedback law up to confidence.

5. Conclusion

In this article, we presented two feedback policy learning algorithms with uniform approximation guarantees — one based on quasi-interpolation and the other on neural networks — for fast computation of control policies in MPC problems. Our approach generates accurate (state, action) data by solving minmax problems exactly, representing a significant departure from traditional synthesis techniques based on multiparametric optimization or kernel methods. Several promising avenues for future work exist; for instance, one could explore the use of physics-informed neural networks or the recently introduced Kolmogorov-Arnold networks for learning approximate policies. Moreover, hardware implementations present an exciting and natural next step that we plan to investigate in subsequent studies.

Appendix A. Preliminaries

A.1. Stability. We provide a very brief background and a definition of ISS-like stability [JW01] which is needed in our study, in particular, to prove closed-loop robust stability results in Theorem 3.8 and Theorem 3.10. Recall the noisy dynamical system defined in (4), and for any continuous admissible feedback $x \mapsto \kappa(x) \in \mathbb{U}$, define the vector field $F(x_t, w_t, v_t) := Ax_t + B\kappa(x_t) + Bv_t + w_t$ and consider the discrete-time system

$$(32) \quad x_{t+1} = F(x_t, w_t, v_t), \quad x_0 = \bar{x}, \quad t \in \mathbb{N}^*.$$

Denote the set of sequences S_w and S_v whose elements are denoted by $\mathbf{w} := (w_t)_{t \in \mathbb{N}}$ and $\mathbf{v} := (v_t)_{t \in \mathbb{N}}$, respectively, such that $w_t \in \mathbb{W}$ and $v_t \in \mathbb{B}_\infty^m[0, \varepsilon]$ for all $t \in \mathbb{N}$. We denote the solution of (32) starting from $\bar{x} \in \mathbb{R}^d$, under the admissible sequence of uncertainties $\mathbf{w} \in S_w$ and $\mathbf{v} \in S_v$ by $x(t; \bar{x}, \mathbf{w}, \mathbf{v})$. Also define $W_{\text{sup}} := \sup_{(w, v) \in \mathbb{W} \times \mathbb{B}_\infty^m[0, \varepsilon]} \|(w, v)\|$.

DEFINITION A.1. Consider the the system (32) and its corresponding notations. Let Ξ be a compact subset of \mathbb{R}^d containing the origin $0 \in \mathbb{R}^d$ in its interior. The set Ξ is *robust positively invariant* for (32) if whenever $x_0 = \bar{x} \in \Xi$, then $x(t; \bar{x}, \mathbf{w}, \mathbf{v}) \in \Xi$ for all $t \in \mathbb{N}^*$.

DEFINITION A.2. [JW01] Given a compact subset Ξ of \mathbb{R}^d containing the origin in its interior, the system (32) with admissible disturbance sequences $(\mathbf{w}, \mathbf{v}) \in S_w \times S_v$ is *ISS-like stable* in Ξ with respect to $(w_t, v_t)_{t \in \mathbb{N}}$ if Ξ is robust positively invariant for (32), and if there exists $\beta(\cdot) \in \mathcal{KL}$ and $\gamma(\cdot) \in \mathcal{K}$ such that for all $\bar{x} \in \Xi$ and $t \in \mathbb{N}^*$

$$(33) \quad \|x(t; \bar{x}, \mathbf{w}, \mathbf{v})\| \leq \beta(\|\bar{x}\|, t) + \gamma(W_{\text{sup}}).$$

A.2. A brief review of the MSA algorithm. Let $n, k \in \mathbb{N}^*$ and consider the convex semi-infinite program (CSIP)

$$(34) \quad \inf_{y \in \Xi} \{\ell(y) \mid \Upsilon(y, \nu) \leq 0 \quad \text{for all } \nu \in \Theta\}$$

where $\Xi \subset \mathbb{R}^n$ is a closed and convex set such that $\text{int } \Xi \neq \emptyset$. The cost $\ell(\cdot)$ is convex and continuous, and the constraint map $\Upsilon(\cdot, \cdot)$ is jointly continuous, and convex in each y for each fixed ν ; $\Theta \subset \mathbb{R}^k$ is compact. By assumption, the interior of the feasible set $\mathcal{H} := \{y \in \Theta \mid \Upsilon(y, \nu) \leq 0 \text{ for all } \nu \in \Theta\}$ is nonempty.

A recent result presented in [DACC22, Theorem 1] offers an efficient method for solving the CSIP (34) with minimal memory usage and serves as the foundation for the data generation process for the learning schemes in this article.

Theorem A.3. [DACC22, Theorem 1] Consider the CSIP (34) along with its associated data and define

$$\mathcal{G}(v_1, \dots, v_n) := \inf_{y \in \Xi} \left\{ \ell(y) \mid \Upsilon(y, v_i) \leq 0 \text{ for } i = 1, \dots, n \right\}.$$

Consider the global maximization problem

$$(35) \quad \sup_{(v_1, \dots, v_n) \in \Theta^n} \mathcal{G}(v_1, \dots, v_n).$$

If $(v_1^*, \dots, v_n^*) \in \Theta^n$ is an optimizer concerning the maximization problem (35), then $G(v_1^*, \dots, v_n^*) = y^*$, where y^* is the optimal value of (34).

A.3. \mathbb{L}_p -norm estimates for ReLU networks. This section collects some of the recent results on \mathbb{L}_p -norm estimates for ReLU networks for $p \in [1, +\infty]$; we shall only employ the $p = +\infty$ case in our work. The first result (Theorem A.4) establishes an explicit rate of approximation obtained via employing ReLU networks for a given function $f \in \mathcal{C}([0, 1]^d)$ in terms of the width W_f and the depth L_f of the network and the dimension $d \in \mathbb{N}^*$.

Theorem A.4. [SYZ22] Let $f \in \mathcal{C}([0, 1]^d)$. For any $W \in \mathbb{N}^*$, $L \in \mathbb{N}^*$, and $1 \leq p \leq +\infty$, there is a function $\hat{f}(\cdot)$ implemented via a ReLU network with width $C_1 \max\{d\lfloor W^{1/d} \rfloor, W + 2\}$ and depth $11L + C_2$ such that

$$(36) \quad \|f(\cdot) - \hat{f}(\cdot)\|_{\mathbb{L}_p([0, 1]^d)} \leq 131\sqrt{d}\omega_f \left(\left(W^2 L^2 \log_3(W + 2) \right)^{-1/d} \right),$$

where $\omega_f(r_0) := \sup_{x, y \in [0, 1]^d} \{|f(x) - f(y)| \mid \|x - y\|_2 \leq r_0\}$ for any $r_0 \geq 0$ is the modulus of continuity for $f(\cdot)$. Moreover, $C_1 = 16$ when $p \in [1, +\infty[$ and 3^{d+3} when $p = +\infty$; $C_2 = 18$ when $p \in [1, +\infty[$ and $18 + 2d$ when $p = +\infty$.

We need similar estimates for Lipschitz functions on $[0, 1]^d$. Observe that for Lipschitz functions $\omega_f(t) = \lambda_f t$, where λ_f is the Lipschitz rank. Then the following *uniform error estimate* follows immediately from Theorem A.4

Corollary A.5. Let $f(\cdot)$ be Lipschitz with rank L_0 defined on $[0, 1]^d$. For any $W \in \mathbb{N}^*$ and $L \in \mathbb{N}^*$ with $W \geq 3^{d+4}d$ and $L \geq 29 + 2d$, there is a function $\hat{f}(\cdot)$ implemented via a ReLU network with width W and depth L such that

$$(37) \quad \|f(\cdot) - \hat{f}(\cdot)\|_{\text{u}} \leq 131\sqrt{d}L_0 \left(\left(\frac{W}{3^{d+5}d} \right)^2 \left(\frac{L-18-2d}{22} \right)^2 \log_3 \left(\frac{W}{3^{d+5}d} + 2 \right) \right)^{-1/d}.$$

Appendix B. Proofs of Lemma 3.1 and Theorem 3.3

PROOF OF LEMMA 3.1.. Consider the SIP (9); for a fixed $W \in \widetilde{\mathbb{W}}^N$, let us define the set

$$\mathcal{S}_{\mathcal{X}} := \{(\theta, \eta, r) \mid \text{Constraints in (9) hold}\}.$$

Notice that $\mathcal{S}_{\mathcal{X}}$ is closed and convex for every $\tilde{w}_t \in \widetilde{\mathbb{W}}$ for all $t = 0, \dots, N-1$. Indeed, $(\theta, \eta, r) \mapsto \mathbb{J}_N(\tilde{x}, \theta, \eta, W) - r$ is convex. The mapping from (θ, η, r) to the solution of the recursion (3), i.e., $(\theta, \eta, r) \mapsto x_{\theta, \eta}(t; \tilde{x}, W)$ and the map $(r, \theta, \eta) \mapsto (u_0, \dots, u_{N-1}) =: U = \theta W + \eta$ is linear in (θ, η) and thus convex [Löf03b, Chapter 7]. Thus the intersection $\mathcal{S} := \bigcap_{W \in \widetilde{\mathbb{W}}^N} \mathcal{S}_{\mathcal{X}}$ is also closed and convex since it is the arbitrary intersection of closed and convex sets. \blacksquare

PROOF OF THEOREM 3.3. Let us show that $\mathcal{G}(\cdot; \bar{x})$ is upper semicontinuous for every $\bar{x} \in X_N$. Consider the relaxed problem (11) corresponding to the original SIP (9), and define the feasible set associated with the (11) by

$$\mathcal{F}(\mathcal{W}; \bar{x}) := \left\{ (\theta, \eta, r) \mid \begin{array}{l} \mathbb{J}_N(\bar{x}, \theta^i, \eta^i, W^i) - r \leq 0, x_N \in \mathbb{M}_F, x(0) = \bar{x}, \\ x_{\theta, \eta}^i(t; \bar{x}, W^i) \in \mathbb{M}, u_t^i + v_t^i \in \mathbb{U}, W^i \in \tilde{\mathbb{W}}^N \end{array} \right\}$$

for $i = 1, \dots, \bar{N}$. The problem (11) is now translated to

$$(38) \quad \mathcal{G}(\mathcal{W}; \bar{x}) := \inf_{(\theta, \eta, r) \in \mathcal{X}} \{r \mid (\theta, \eta, r) \in \mathcal{F}(\mathcal{W}; \bar{x})\}.$$

Observe that:

- (P1) the map $(\theta, \eta, r) \mapsto \mathbb{J}_N(\bar{x}, \theta, \eta, W) - r$ is continuous in (θ, η, r) ;
- (P2) the map $(\theta, \eta, r) \mapsto \theta W + \eta$ is continuous in (θ, η, r) ;
- (P3) the map $(\theta, \eta, r) \mapsto x_{\theta, \eta}(t; \bar{x}, W)$ is continuous in (r, θ, η) for all $t = 0, \dots, N-1$.

Fix $(\bar{\theta}, \bar{\eta}, \bar{r}, \tilde{\mathcal{W}}) \in \mathcal{X} \times \tilde{\mathbb{W}}^{\bar{N}}$, where $(\bar{\theta}, \bar{\eta}, \bar{r}) \in \mathcal{F}(\tilde{\mathcal{W}}; \bar{x})$. Invoking Assumption 3.2 and the continuity of the maps in (P1)–(P3), there exists a sequence $(\bar{\theta}_n, \bar{\eta}_n, \bar{r}_n)_{n \in \mathbb{N}} \subset \mathcal{F}(\tilde{\mathcal{W}}; \bar{x})$ such that $(\bar{\theta}_n, \bar{\eta}_n, \bar{r}_n)_{n \in \mathbb{N}} \rightarrow (\bar{\theta}, \bar{\eta}, \bar{r})$ as $n \rightarrow +\infty$. This immediately implies that the constraint qualification condition (CQ) in [Sti18, Definition 5.3, pp 53] is satisfied, i.e., for every $\bar{x} \in X_N$ the following hold: $(\bar{\theta}_n, \bar{\eta}_n, \bar{r}_n) \in \text{int } \mathcal{F}(\tilde{\mathcal{W}}; \bar{x})$. Upper semicontinuity of $\tilde{\mathbb{W}}^{\bar{N}} \ni \mathcal{W} \mapsto \mathcal{G}(\mathcal{W}; \bar{x}) \in \mathbb{R}$ now follows readily by invoking [Sti18, Lemma 5.4-(b), p. 54].

The existence of an optimizer $\mathcal{W}^* \in \tilde{\mathbb{W}}^{\bar{N}}$ follows immediately from the upper semicontinuity of $\mathcal{G}(\cdot; \bar{x})$ from (3.3-a), compactness of $\tilde{\mathbb{W}}^{\bar{N}}$, and from the Weierstrass Theorem, thereby proving (3.3-b).

From the Assumption 3.2 there exists a pair $(\theta, \eta, r) \in \mathcal{X}$ such that for all $\mathcal{W} \in \tilde{\mathbb{W}}^{\bar{N}}$, the interior of the set $\bigcap_{(W^i)_{i \in [1, \bar{N}]}} \mathcal{S}_{\mathcal{X}}$ is nonempty. Moreover, in the decision and semi-infinite variable pair, the constraint maps are jointly continuous. Indeed the maps $(\theta, \eta, r, W) \mapsto x_{\theta, \eta}(t; \bar{x}, W)$ and the map $(r, \theta, \eta, W) \mapsto (u_0, \dots, u_{N-1}) =: U = \theta W + \eta$ are continuous and consequently $(\theta, \eta, r, W) \mapsto \mathbb{J}_N(\bar{x}, \theta, \eta, W) - r$ is continuous (recall that $c(\cdot, \cdot)$ was jointly continuous). Then Lemma 3.1, the problem data (1-a)–(1-d) and Theorem A.3 assures that there exists an optimizer $\mathcal{W}^* \in \tilde{\mathbb{W}}^{\bar{N}}$ such that

$$\mathbb{J}_N^*(\bar{x}) = \mathcal{G}(\mathcal{W}^*; \bar{x}) \text{ for every } \bar{x} \in X_N,$$

which completes the proof. \blacksquare

Appendix C. Proofs of Theorem 3.8 and Theorem 3.10

PROOF OF THEOREM 3.8. We begin by giving a proof of the first assertion. Fix $\varepsilon > 0$ and $\psi(\cdot) \in \mathcal{S}(\mathbb{R}^d)$ satisfying moment condition of order M and decay condition of order $K > d$, with C_0 as the upper bound in (16). Recall the approximation schemes (14) and (19). Then we have the estimate (see (17))

$$(39) \quad \|\widehat{\mu}_0(\cdot) - \mu_0^*(\cdot)\|_{\mathbb{u}} \leq C_{\gamma} L_0 h \sqrt{\mathcal{D}} + \Delta_0(\psi, \mathcal{D}) \text{ on } \mathbb{R}^d,$$

where $\mu_0^*(\cdot)$ is the extended policy (13) (which is Lipschitz continuous with rank L_0), the quantity $\Delta_0(\psi, \mathcal{D}) := \mathcal{E}_0(\psi, \mathcal{D}) \|\mu_0^*(\cdot)\|_{\mathbb{u}}$ is the saturation error, the term $\mathcal{E}_0(\psi, \mathcal{D})$ and C_{γ} are defined below (17). From [MS07, Chapter 2, Corollary 2.13] it follows that for the preassigned $\varepsilon > 0$, we can find $\mathcal{D}_{\min} > 0$ such that whenever $\mathcal{D} \geq \mathcal{D}_{\min}$, we have $\mathcal{E}_0(\psi, \mathcal{D}) \leq \frac{\varepsilon}{3 \|\mu_0^*(\cdot)\|_{\mathbb{u}}}$. Fixing such a $\mathcal{D} \geq \mathcal{D}_{\min}$, we ensure that $\Delta_0(\psi, \mathcal{D}) \leq \frac{\varepsilon}{3}$. Fixing

$$(40) \quad h = \frac{\varepsilon}{3 C_{\gamma} L_0 \sqrt{\mathcal{D}}},$$

from (39) we arrive immediately at $\|\mu_0^*(\cdot) - \widehat{\mu}_0(\cdot)\|_{\text{u}} \leq \frac{2\varepsilon}{3}$. We also have the estimate [MS07, §2.3.2, eq. (2.57)]

$$(41) \quad \|\mu_0^\dagger(x) - \widehat{\mu}_0(x)\| \leq \mathcal{B} \left(\frac{\sqrt{\mathcal{D}}}{\rho} \right)^{K-d} \|\widehat{\mu}_0(\cdot)\|_{\text{u}}$$

for all $x \in \mathbb{R}^d$, where \mathcal{B} is a constant specific to $\psi(\cdot)$. In view of (41) we pick

$$\rho := \sqrt{\mathcal{D}} \left(\frac{\varepsilon}{3\mathcal{B} \|\mu_0^*(\cdot)\|_{\text{u}}} \right)^{1/(d-K)}.$$

Then $\|\widehat{\mu}_0(x) - \mu_0^\dagger(x)\| \leq \frac{\varepsilon}{3}$ for all $x \in \mathbb{R}^d$. Now restricting the domains of $\mu_0^*(\cdot)$, $\widehat{\mu}_0(\cdot)$, and $\mu_0^\dagger(\cdot)$ to X_N while retaining the same notation for all of them, we see that

$$(42) \quad \begin{aligned} \|\mu_0^*(x) - \mu_0^\dagger(x)\| &\leq \|\mu_0^*(x) - \widehat{\mu}_0(x)\| + \|\widehat{\mu}_0(x) - \mu_0^\dagger(x)\| \\ &\leq C_\gamma L_0 h \sqrt{\mathcal{D}} + \Delta_0(\psi, \mathcal{D}) + \mathcal{B} \left(\frac{\sqrt{\mathcal{D}}}{\rho} \right)^{K-d} \|\mu_0^*(\cdot)\|_{\text{u}} \leq \frac{2\varepsilon}{3} + \frac{\varepsilon}{3} = \varepsilon. \end{aligned}$$

In summary, since $\varepsilon > 0$ was preassigned and we picked $(h, \mathcal{D}, \rho) \in]0, +\infty[^3$ such that the estimate (42) holds, the first assertion (3.8-a) stands established.

We proceed to prove the second assertion (3.8-b) concerning stability of the closed loop process $(x_t)_{t \in \mathbb{N}}$ corresponding to the system (1) under the approximate feedback $\mu_0^\dagger(\cdot)$. Under $\mu_0^\dagger(\cdot)$, the closed loop process is given by:

$$(43) \quad x^+ = Ax + B\mu_0^\dagger(x) + w,$$

where x^+ denotes the next state when the current state is x . Recall that the (state-dependent) approximation noise is given by $v := \mu_0^\dagger(x) - \mu_0^*(x)$. Then from (43) we have

$$(44) \quad \begin{aligned} x^+ &= Ax + B\mu_0^\dagger(x) - B\mu_0^*(x) + B\mu_0^*(x) + w = Ax + B(\mu_0^\dagger(x) - \mu_0^*(x)) + B\mu_0^*(x) + w \\ &= Ax + B\mu_0^*(x) + B\zeta + w. \end{aligned}$$

Notice that the closed-loop dynamics (44) is essentially the noisy system (3) under the policy $\mu_0^*(\cdot)$, which, under Assumption 3.6 is stable in the sense of Definition A.2 and the ensuing optimal control problem (6) is recursively feasible; see [MF19, §3]. This immediately proves ISS-like stability of the system (1) under the approximate feedback policy $\mu_0^\dagger(\cdot)$ under the equivalence established in (44) (i.e., stability of the system (43)) in the sense of Definition A.2. ■

PROOF OF THEOREM 3.10.. We first prove the error estimate (3.10-a), and to this end, fix $\varepsilon > 0$. Recall that the policy $\mu_0^*(\cdot)$ is Lipschitz continuous and L_0 is its minimal Lipschitz rank, and the ReLU-NN approximate feedback policy is given by $\mu_0^\dagger(\cdot)$. Recalling the estimate (37) in Corollary A.5, we introduce the simplified notations $\tilde{L} := \frac{L-18-2d}{22}$, where L denotes the depth of the neural network, and $\tilde{W} := \frac{W}{3^{d+5}d}$, where W represents the network's width. With these definitions, we reformulate the estimate (37), replacing $f(\cdot)$ and $f_{\text{ReLU}}(\cdot)$ with $\mu_0^*(\cdot)$ and $\mu_0^\dagger(\cdot)$, respectively. Then we have the estimate

$$(45) \quad \|\mu_0^*(\cdot) - \mu_0^\dagger(\cdot)\|_{\text{u}} \leq 131\sqrt{d}L_0 \left(\tilde{W}^2 \tilde{L}^2 \log_3(\tilde{W} + 2) \right)^{-\frac{1}{d}},$$

To ensure that the right-hand side of (45) remains bounded by ε , we must appropriately determine the parameters within \tilde{L} and \tilde{W} . Since the dimension d is fixed, assigning a specific value $W = \mathcal{W}_0$ to the width of the ReLU network uniquely determines \tilde{W} . We then proceed by selecting

$$(46) \quad \tilde{L} := \sqrt{\frac{\varepsilon^{-d}}{(131\sqrt{d}L_0)^{-d}\tilde{W}^2 \log_3(\tilde{W} + 2)}}.$$

Substituting (46) in (45), we get

$$(47) \quad \left\| \mu_0^*(\cdot) - \mu_0^\dagger(\cdot) \right\|_{\text{u}} \leq 131\sqrt{d}L_0 \left(\tilde{W}^2 \frac{\varepsilon^{-d} \log_3(\tilde{W} + 2)}{(131\sqrt{d}L_0)^{-d}\tilde{W}^2 \log_3(\tilde{W} + 2)} \right)^{-1/d} = \varepsilon,$$

and the value for L can then be calculated as $L = \lceil 22\tilde{L} + 18 + 2d \rceil$. Thus, given a preassigned $\varepsilon > 0$ and a fixed width $W = \mathcal{W}_0 \in \mathbb{N}^*$, we find $L \in \mathbb{N}^*$ such that the criterion of uniform ε -tolerance is respected, and the assertion (3.10-a) follows.

We now proceed to prove assertion (3.10-b). In the same spirit, given $L = \mathcal{L}_0$ for the depth of the neural network, $\tilde{L} = \frac{\mathcal{L}_0 - 18 - 2d}{22}$ gets fixed. Now we set

$$(48) \quad \tilde{W} := 3 \left[\frac{\varepsilon^{-d}}{(131\sqrt{d}L_0)^{-d}\tilde{L}^2} \right]^{1/3} - 1.$$

By leveraging the bounds $\log_3(x+1) \leq x$ and $\log_3(x+2) \geq \log_3(x+1)$, we can reformulate (45) in an alternative form. This allows us to express the error estimate in a manner that facilitates further analysis. Specifically, we rewrite it as

$$(49) \quad \begin{aligned} \left\| \mu_0^*(\cdot) - \mu_0^\dagger(\cdot) \right\|_{\text{u}} &\leq 131\sqrt{d}L_0 \left(\left(\tilde{W}^2 \tilde{L}^2 \log_3(\tilde{W} + 2) \right)^{-\frac{1}{d}} \right) \\ &\leq 131\sqrt{d}L_0 \left(\left(\tilde{L}^2 [\log_3(\tilde{W} + 1)]^3 \right)^{-\frac{1}{d}} \right), \end{aligned}$$

and substituting (48) in (49), we get

$$(50) \quad \left\| \mu_0^*(\cdot) - \mu_0^\dagger(\cdot) \right\|_{\text{u}} \leq 131\sqrt{d}L_0 \left(\left(\frac{\varepsilon^{-d}}{(131\sqrt{d}L_0)^{-d}\tilde{L}_0^2} \right) \tilde{L}_0^2 \right)^{-1/d} = \varepsilon.$$

From \tilde{W} we find the width $W = \lceil 3^{d+5} d \tilde{W} \rceil$ of the neural network. We have shown that given $\varepsilon > 0$ and a fixed $\mathcal{L}_0 \in \mathbb{N}^*$, we can find a $W \in \mathbb{N}^*$ such that the given tolerance is respected, and assertion (3.10-b) stands established.

Finally, (3.10-c) follows verbatim from the proof in §3.3 because the uniform error estimates (47) and (50) hold. \blacksquare

References

- [ACB20] P. K. Mishal Assif, D. Chatterjee, and R. Banavar, *Scenario approach for minmax optimization with emphasis on the nonconvex case: Positive results and caveats*, SIAM Journal on Optimization **30** (2020), no. 2, 1119–1143, doi: <https://doi.org/10.1137/19M1271026>.
- [ApS19] MOSEK ApS, *The MOSEK optimization toolbox for MATLAB manual. version 9.0.*, 2019.
- [BB08] T. Başar and P. Bernhard, *H_∞ Optimal Control and Related Minimax Design Problems: A Dynamic Game Approach*, Springer Science & Business Media, 2008, doi: <https://doi.org/10.1007/978-0-8176-4757-5>.
- [BVP⁺12] H. Borhan, A. Vahidi, A. M. Phillips, M. L. Kuang, I. V. Kolmanovsky, and S. Di Cairano, *MPC-based energy management of a power-split hybrid electric vehicle*, IEEE Transactions on Control Systems Technology **20** (2012), no. 3, 593–603, doi: [10.1109/TCST.2011.2134852](https://doi.org/10.1109/TCST.2011.2134852).
- [CKK⁺08] P. Cortés, M. P. Kazmierkowski, R. M. Kennel, D. E. Quevedo, and J. Rodríguez, *Predictive control in power electronics and drives*, IEEE Transactions on industrial electronics **55** (2008), no. 12, 4312–4324, doi: <https://doi.org/10.1109/TIE.2008.2007480>.
- [DACC22] S. Das, A. Aravind, A. Cherukuri, and D. Chatterjee, *Near-optimal solutions of convex semi-infinite programs via targeted sampling*, Annals of Operations Research (2022), doi: <https://doi.org/10.1007/s10479-022-04810-4>.
- [DHP21] R. DeVore, B. Hanin, and G. Petrova, *Neural network approximation*, Acta Numerica **30** (2021), 327–444, doi: [10.1017/S0962492921000052](https://doi.org/10.1017/S0962492921000052).
- [Don21] A. L. Dontchev, *Lectures on Variational Analysis*, vol. 205, Applied Mathematical Sciences, Springer Cham, 2021, doi: <https://doi.org/10.1007/978-3-030-79911-3>.

[GC12] Y. Gao and K. T. Chong, *The explicit constrained min-max model predictive control of a discrete-time linear system with uncertain disturbances*, IEEE Transactions on Automatic Control **57** (2012), no. 9, 2373–2378, doi: [10.1109/TAC.2012.2186090](https://doi.org/10.1109/TAC.2012.2186090).

[GC24] S. Ganguly and D. Chatterjee, *Exact solutions to minmax optimal control problems for constrained noisy linear systems*, IEEE Control Systems Letters **8** (2024), 2063–2068, doi: <https://doi.org/10.1109/LCSYS.2024.3439208>.

[GC25] ———, *Explicit feedback synthesis driven by quasi-interpolation for nonlinear model predictive control*, IEEE Transactions on Automatic Control **70** (2025), no. 7, 1–8, doi: [10.1109/TAC.2025.3538767](https://doi.org/10.1109/TAC.2025.3538767).

[GDC24] S. Ganguly, R. A. D’Silva, and D. Chatterjee, QuITO v.2: *Trajectory optimization with uniform error guarantees under path constraints*, 2024, url: <https://arxiv.org/abs/2404.13681>.

[HKTA18] M. Hertneck, J. Köhler, S. Trimpe, and F. Allgöwer, *Learning an approximate model predictive controller with guarantees*, IEEE Control Systems Letters **2** (2018), no. 3, 543–548, doi: [10.1109/LCSYS.2018.2843682](https://doi.org/10.1109/LCSYS.2018.2843682).

[HPM06] S. Har-Peled and M. Mendel, *Fast construction of nets in low-dimensional metrics and their applications*, SIAM Journal on Computing **35** (2006), no. 5, 1148–1184, doi: <https://doi.org/10.1137/S0097539704446281>.

[JW01] Z.-P. Jiang and Y. Wang, *Input-to-state stability for discrete-time nonlinear systems*, Automatica **37** (2001), no. 6, 857–869, doi: [https://doi.org/10.1016/S0005-1098\(01\)00028-0](https://doi.org/10.1016/S0005-1098(01)00028-0).

[Kha02] H. K. Khalil, *Nonlinear Systems*, Prentice Hall, New Jersey, 2002.

[KL20] B. Karg and S. Lucia, *Efficient representation and approximation of model predictive control laws via deep learning*, IEEE Transactions on Cybernetics **50** (2020), no. 9, 3866–3878, doi: <https://doi.org/10.1109/TCYB.2020.2999556>.

[KSAS17] M. Kamel, T. Stastny, K. Alexis, and R. Siegwart, *Model predictive control for trajectory tracking of unmanned aerial vehicles using robot operating system*, Robot Operating System (ROS) The Complete Reference (Volume 2) (2017), 3–39, doi: https://doi.org/10.1007/978-3-319-54927-9_1.

[Löf03a] J. Löfberg, *Approximations of closed-loop minimax MPC*, 42nd IEEE International Conference on Decision and Control, vol. 2, 2003, doi: [10.1109/CDC.2003.1272813](https://doi.org/10.1109/CDC.2003.1272813), pp. 1438–1442 Vol.2.

[Löf03b] ———, *Minimax Approaches to Robust Model Predictive Control*, Ph.D. thesis, Linköping University, 2003, URL: <https://rt.isy.liu.se/research/reports/Ph.D.Thesis/PhD812.pdf>.

[Löf04] ———, *YALMIP: A toolbox for modeling and optimization in MATLAB*, 2004 IEEE international conference on robotics and automation, 2004, doi: <https://doi.org/10.1109/CACSD.2004.1393890>, pp. 284–289.

[Löf12] ———, *Automatic robust convex programming*, Optimization Methods and Software **27** (2012), no. 1, 115–129, doi: <https://doi.org/10.1080/10556788.2010.517532>.

[Loj88] S. Lojasiewicz, *An Introduction to the Theory of Real Functions*, third ed., A Wiley-Interscience Publication, John Wiley & Sons, Ltd., Chichester, 1988, With contributions by M. Kosiek, W. Mlak and Z. Opial, Translated from the Polish by G. H. Lawden.

[MDM12] S. Mariethoz, A. Domahidi, and M. Morari, *High-bandwidth explicit model predictive control of electrical drives*, IEEE Transactions on Industry Applications **48** (2012), no. 6, 1980–1992, doi: [10.1109/TIA.2012.2226198](https://doi.org/10.1109/TIA.2012.2226198).

[MF19] D. Q. Mayne and P. Falugi, *Stabilizing conditions for model predictive control*, International Journal of Robust and Nonlinear Control **29** (2019), no. 4, 894–903, doi: <https://doi.org/10.1002/rnc.4409>.

[MRLSO19] A. Marquez-Ruiz, M. Loonen, M. B. Saltik, and L. Özkan, *Model learning predictive control for batch processes: A reactive batch distillation column case study*, Industrial & Engineering Chemistry Research **58** (2019), no. 30, 13737–13749, doi: <https://doi.org/10.1021/acs.iecr.8b06474>.

[MS07] V. G. Maz’ya and G. Schmidt, *Approximate Approximations*, Mathematical Surveys and Monographs, vol. 141, American Mathematical Society, Providence, RI, 2007, doi: <https://doi.org/10.1090/surv/141>.

[PM20] J. A. Paulson and A. Mesbah, *Approximate closed-loop robust model predictive control with guaranteed stability and constraint satisfaction*, IEEE Control Systems Letters **4** (2020), no. 3, 719–724, doi: [10.1109/LCSYS.2020.2980479](https://doi.org/10.1109/LCSYS.2020.2980479).

[PZ95] T. Parisini and R. Zoppoli, *A receding-horizon regulator for nonlinear systems and a neural approximation*, Automatica **31** (1995), no. 10, 1443–1451, doi: [https://doi.org/10.1016/0005-1098\(95\)00044-W](https://doi.org/10.1016/0005-1098(95)00044-W).

[Sti18] G. Still, *Lectures on Parametric Optimization: An Introduction*, Optimization Online (2018), URL: <https://optimization-online.org/?p=15154>.

[SYZ22] Z. Shen, H. Yang, and S. Zhang, *Optimal approximation rate of ReLU networks in terms of width and depth*, Journal de Mathématiques Pures et Appliquées **157** (2022), 101–135, doi: <https://doi.org/10.1016/j.matpur.2021.07.009>.

- [WCW⁺24] Z. Wu, P. D. Christofides, W. Wu, Y. Wang, F. Abdullah, A. Alnajdi, and Y. Kadakia, *A tutorial review of machine learning-based model predictive control methods*, Reviews in Chemical Engineering (2024), no. 0, doi: <https://doi.org/10.1515/revce-2024-0055>.
- [WHL22] E. Weinan, J. Han, and J. Long, *Empowering optimal control with machine learning: A perspective from model predictive control*, IFAC-PapersOnLine **55** (2022), no. 30, 121–126, doi: <https://doi.org/10.1016/j.ifacol.2022.11.039>.
- [WWTW24] W. Wang, Y. Wang, Y. Tian, and Z. Wu, *Explicit machine learning-based model predictive control of nonlinear processes via multi-parametric programming*, Computers & Chemical Engineering **186** (2024), 108689, doi: <https://doi.org/10.1016/j.compchemeng.2024.108689>.
- [WZW⁺24] W. Wang, H. Zhang, Y. Wang, Y. Tian, and Z. Wu, *Fast explicit machine learning-based model predictive control of nonlinear processes using input convex neural networks*, 2024, doi: <https://arxiv.org/abs/2408.06580>.
- [XL19] Y. Xi and D. Li, *Predictive Control: Fundamentals and Developments*, John Wiley & Sons, 2019, doi: <https://doi.org/10.1002/9781119119593>.